Geophys. J. Int. (1998) **133,** 585–606

On two-dimensional interpretation of magnetotelluric soundings

M. N. Berdichevsky, V. I. Dmitriev and E. E. Pozdnjakova

Geological Department and Department of Computing Mathematics, Moscow State University, Vorob'evy Gory, Moscow, 119899, *Russia.*
E-mail: berd@geo.geol.msu.su

Accepted 1997 November 18. Received 1997 November 17; in original form 1995 September 28

SUMMARY

The paper presents the views of the 2-D interpretation of magnetotelluric (MT) data that are characteristic of the Russian magnetotelluric school. Discussing the strategy of 2-D interpretation of MT data, we have to answer three questions. In decreasing order of importance, these questions are as follows. (1) Which field mode is more sensitive to the near-surface and deep structures that are the targets of MT surveys? (2) Which field mode is more robust to the 3-D effects caused by real geological bodies? (3) Which field mode is more susceptible to the static shift induced by near-surface inhomogeneities?

We examine the transverse magnetic (TM) and transverse electric (TE) modes of the 2-D magnetotelluric field and show that they satisfy the principle of information complementarity: (1) while the TM mode is more sensitive to the near-surface structures, the TE mode may be more sensitive to the deep structures; (2) while the TM mode is more robust to the 3-D effects caused by conductive structures, the TE mode may be more robust to the 3-D effects caused by resistive structures; and (3) while the TM mode is more susceptible to the static shift, the TE mode may be almost undistorted. Thus, the gaps left by one mode can be filled by another mode. If so, the most comprehensive and reliable information on the conductivity of the Earth's interior can be obtained using both modes, i.e. the transverse and longitudinal MT curves.

The general scheme of this bimodal MT inversion is rather simple. The transverse curves provide details of near-surface structures (e.g. in the sediments) and allow one to evaluate the lithosphere resistance and outline the deep conductive faults, while the longitudinal curves help one to detect the conductive zones in deep layers of the lithosphere and in the asthenosphere. An efficient two-level algorithm for the bimodal MT inversion realizing this scheme is suggested. As an illustration, the paper presents the geoelectrical model of the Kirghiz Tien Shan constructed by means of the bimodal MT inversion

Key words: 2-D inversion, magnetotellurics.

INTRODUCTION

It is a matter of common knowledge that the 2-D magnetotelluric field consists of the TM and TE modes. The TM mode is related to the *B*-polarized wave generating the transverse MT curves (telluric current flows across the structures), and the TE mode is related to the *E*-polarized wave generating the longitudinal MT curves (telluric current flows along the structures). The main difference between these modes is that the TM mode charges the structures, and its anomalies are of galvanic nature, but the TE mode does not charge the structures, and its anomalies are of inductive nature.

The TM and TE modes offer different sensitivities to near-surface and deep structures and provide different accuracies of 2-D approximation of real 3-D bodies. These properties of the TM and TE modes dictate the philosophy and practical strategy of the 2-D interpretation of MT data collected in regions with elongated structures.

The problems of 2-D interpretation of magnetotelluric soundings have been discussed in many papers and monographs (Svetov 1973; Kaufman 1974; Berdichevsky & Dmitriev 1976a; Jupp & Vozoff 1977; Kaufman & Keller 1981; Veselovsky & Yudin 1988; Park, Orange & Madden 1983; Wannamaker, Hohman & Ward 1984; Berdichevsky & Zhdanov 1984; Park 1985; Mackie, Bennet & Madden 1988; Wannamaker *et al.* 1989; Wannamaker *et al.* 1991; Park *et al.* 1991; Berdichevsky,

Koldayev & Jakovlev 1992; Weaver 1994; Zhdanov & Keller 1994; Berdichevsky, Dmitriev & Kuznetsov 1995; Gupta & Jones 1995; Banks *et al.* 1996). The discussion exhibits a wide range of various and sometimes conflicting viewpoints, from 'the TM-impedance functions are emphasized because theory and experiment show that they are more robust to 3-D effects' (Wannamaker *et al.* 1989) to 'inverting both the TE and TM modes simultaneously results in models which fit the TM locally without resolving large-scale structure evinced only by the TE mode' (Banks *et al.* 1996).

In this paper we attempt to establish some general principles of bimodal MT inversion. The paper is based on the magnetotelluric experience gained in different geological provinces of Russia and the former Soviet Union (more than 10 000 MT soundings in the last three decades). All models given in the paper have been calculated using finite-element and integral-equation solutions (Wannamaker, Stodt & Rijo 1987; Dmitriev & Pozdnjakova 1991). Throughout the paper we use the terms 'TE' and 'TM' for the field modes in the ideal 2-D models, and the terms 'longitudinal' ('L') and 'transverse' ('T') for MT curves obtained with the polarization of the electrical field along and across the ideal 2-D or elongated 3-D structure. For the sake of consistency we begin with a brief overview of the properties of the 2-D magnetotelluric field.

SENSITIVITY OF THE TE AND TM MODES

Consider two basic lithosphere models consisting of an upper conductive layer (the sedimentary cover), intermediate resistive layers (the consolidated crust and upper mantle) and a conductive basement (the asthenosphere).

Fig. 1 shows model A, with a 2-D, narrow, horst-like resistive elevation in the sediments. This shallow structure is clearly marked by all graphs of the transverse apparent resistivity calculated for periods from 0.1 to 10 000 s, but is barely perceptible in the corresponding graphs of the longitudinal apparent resistivity.

Fig. 2 depicts the apparent resistivity curves ρ_A(2-D, TM), ρ_A(2-D, TE) and the impedance phase curves φ(2-D, TM), φ(2-D, TE) obtained at the central site O, just above the horst. Compare these curves with the 1-D curves ρ_A(1-D, O), φ(1-D, O) and ρ_A(1-D, R), φ(1-D, R), which stand for the normal curves at site O and the remote site R. We see that (1) the ascending branch of the ρ_A(2-D, TM) curve coincides with the normal ρ_A(1-D, O) curve, but its descending branch departs from the ρ_A(1-D, O) curve and is dramatically shifted upwards, reflecting a fall in the conductance S of the upper layer (the static shift, S effect); (2) the ascending branch of the ρ_A(2-D, TE) curve gravitates to the remote ρ_A(1-D, R) curve, and its descending branch is not shifted; (3) the high-frequency and low-frequency branches of the φ(2-D, TM) curve merge with the normal φ(1-D, O) curve; and (4) the φ(2-D, TE) curve, over a wide range of frequencies, coincides with the φ(1-D, R) curve.

It is evident that the TM impedance is more sensitive to near-surface resistive structures than the TE impedance. The horst can easily be indicated using the TM mode, but it may be missed while using the TE mode

Now let us come to the 2-D model B, with uniform sediments, a high-ohmic lithosphere of resistivity ρ_L and a broad trapezoidal elevation of the conductive asthenosphere (Fig. 3). It is known that the TM response of a buried bounded

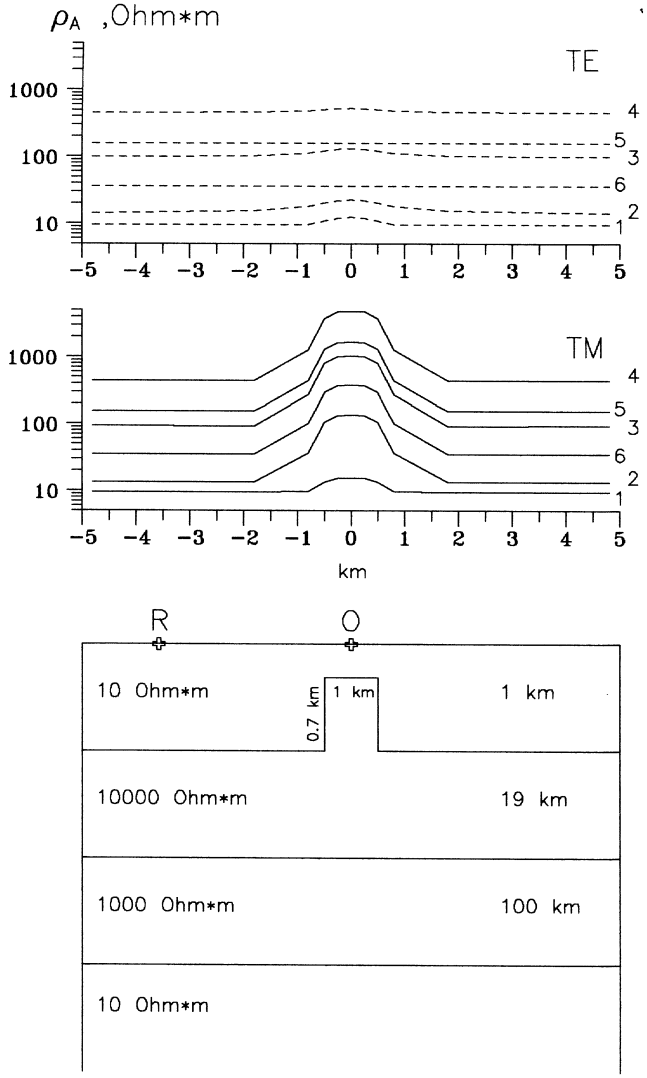

Figure 1. Model A: a 2-D horst-like resistive elevation in the sedimentary cover. Top: apparent resistivity profiles for the TE and TM modes. Curves 1, period $T = 0.1$ s; 2, 1 s; 3, 10 s; 4, 100 s; 5, 1000 s; 6, 10 000 s. Bottom: cross-section of the model (not to scale); O, R, sounding sites.

conductor (crustal or mantle) depends on its width w and adjustment distance $d = \sqrt{S_S R_L}$, calculated from the sediment conductance $S_S = h_S/\rho_S$ and the overlying lithosphere resistance $R_L = h_L\rho_L$, where h_S and h_L are the thicknesses of sediments and lithosphere, respectively (Berdichevsky & Jakovlev 1990). The crucial factor is the ratio w/d that defines the galvanic connection between the sediments and the deep conductor controlling the vertical redistribution of TM currents. The smaller this ratio, the weaker the effect of the deep conductor. With $w/d \ll 1$ a deep conductor is fully screened. In the model considered here, $S_S = 100$ S and the minimum R_L is $5 \times 10^9\ \Omega\,m^2$. In this model, typical for many regions of our planet, the minimum adjustment distance is 700 km, so that $w/d < 0.21$. It means that the mechanism of vertical redistribution of TM currents is inoperative here. No wonder that the asthenosphere elevation is not reflected in the graphs of transverse apparent resistivity, whose anomalies are of galvanic nature (the intensive screening effect!). At the same time this

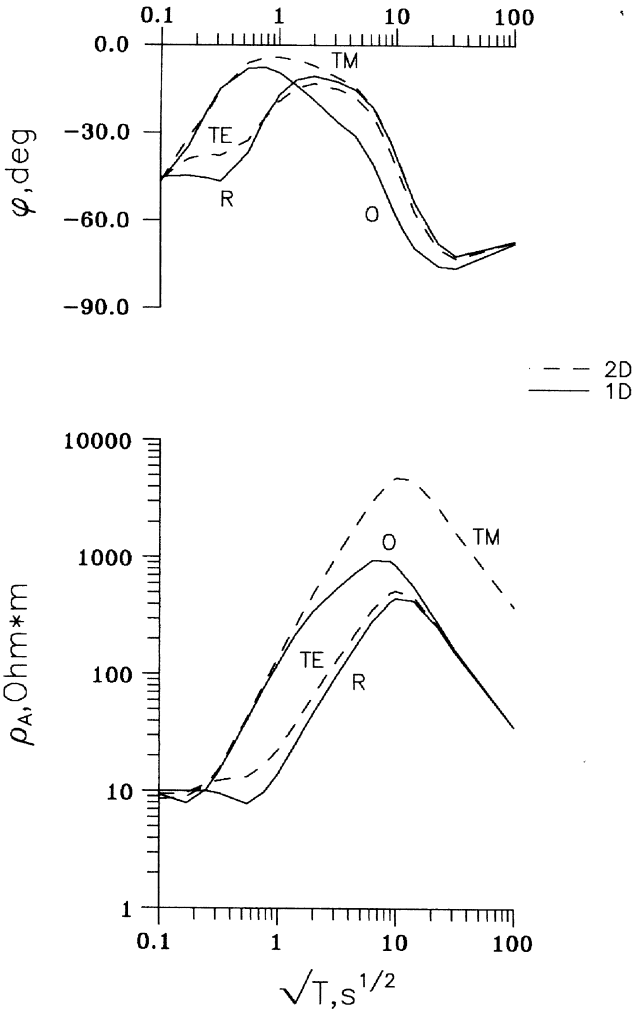

Figure 2. Apparent resistivity and impedance phase curves in model A. Solid lines: 1-D curves at central site O and remote site R; dashed lines: 2-D curves for the TE and TM modes at central site O.

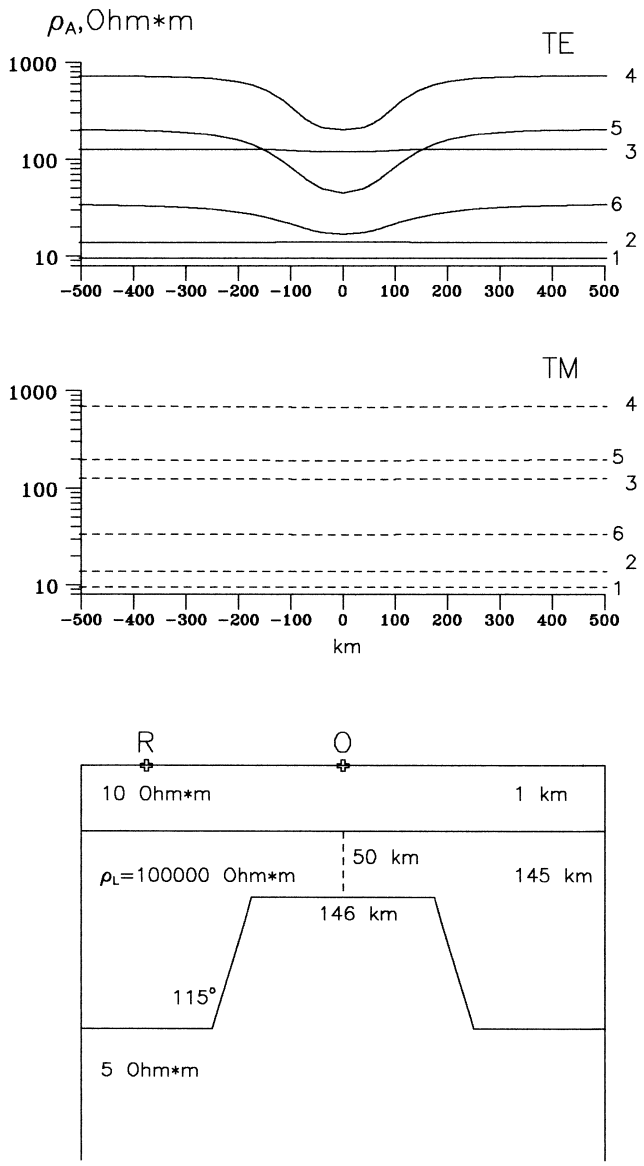

Figure 3. Model B: a 2-D elevation of the conductive asthenosphere. Top: apparent resistivity profiles for TE and TM modes, $\rho_L = 100\,000\ \Omega$ m. Curves 1, period $T = 0.1$ s; 2, 1 s; 3, 10 s; 4, 100 s; 5, 1000 s; 6, 10 000 s. Bottom: cross-section of the model (not to scale); ρ_L, lithosphere resistivity; O, R, sounding sites.

deep structure is clearly marked by the graphs of low-frequency longitudinal resistivity, whose anomalies are of inductive nature. It is evident that the TE impedance is more sensitive to deep conductive structures than the TM impedance is. So, the asthenosphere elevation can be indicated using the TE mode, but it may be missed while using the TM mode.

Fig. 4 shows the apparent resistivity and impedance phase curves ρ_A(2-D, TM), φ(2-D, TM) and ρ_A(2-D, TE), φ(2-D, TE) calculated for different lithosphere resistivities ρ_L. The curves were obtained at the central site O above the asthenosphere elevation. Compare these curves with the 1-D ('normal') curves ρ_A(1-D, O), φ(1-D, O) and ρ_A(1-D, R), φ(1-D, R), related to the central site O and remote site R. In the case $\rho_L = 100\,000\ \Omega$ m we have $w/d < 0.21$. Note that here the curves ρ_A(2-D, TM) and φ(2-D, TM) coincide with the remote normal curves ρ_A(1-D, R) and φ(1-D, R). They virtually ignore the asthenosphere elevation. In contrast to this, the ρ_A(2-D, TE) and φ(2-D, TE) curves have low-frequency descending branches that lie along the normal curves ρ_A(1-D, O) and φ(1-D, O). They demonstrate a pronounced impact of the asthenosphere elevation. In the case $\rho_L = 1000\ \Omega$ m the minimum ratio w/d is 2.1. Here the curves ρ_A(2-D, TE) and φ(2-D, TE) practically do not vary, while the curves ρ_A(2-D, TM) and φ(2-D, TM) deviate from the ρ_A(1-D, R) and φ(1-D, R) curves and approach the ρ_A(1-D, O) and φ(1-D, O) curves. Now the transverse curves do reflect (though with great smoothing) the asthenosphere elevation. It is evident that the TM impedance is more sensitive to the lithosphere resistance than the TE impedance is.

ROBUSTNESS OF THE TM AND TE MODES

What is the accuracy of 2-D approximation of real 3-D structures? This question was considered in the pioneering works of Svetov (1973) and Kaufman (1974). One of the most interesting developments in the succeeding years was the paper by Wannamaker *et al.* (1984), which gave an elegant theory of 3-D effects and examined some 3-D models describing the MT field in the Basin and Range province.

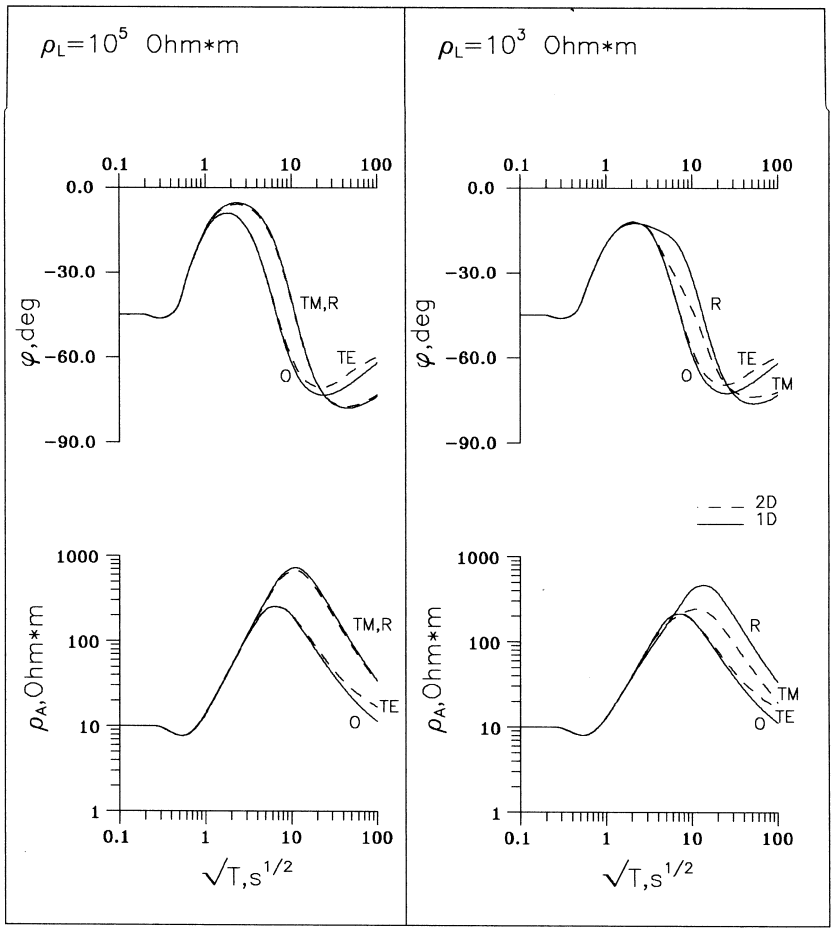

Figure 4. Apparent resistivity and impedance phase curves in model B; ρ_L, resistivity of the lithosphere. Solid lines: 1-D curves at central site O and remote site R; dashed lines: 2-D curves for the TE and TM modes at central site O.

Following Wannamaker and co-authors, consider model C, with an elongated 3-D prism of resistivity ρ_P located in the first layer, which is of resistivity $\rho_S = 400\ \Omega$ m (Fig. 5). The prism length and width are $l = 35$ km and $w = 15$ km, and its elongation is $e = l/w = 2.3$.

We shall begin with the conductive prism ($\rho_P \ll \rho_S$) that was considered by Wannamaker *et al.* (1984). Let $\rho_P = 2\ \Omega$ m. This model simulates a valley. On the left-hand side of Fig. 6 we show the 3-D curves of ρ_A(3-D) related to the central point O. They are labelled L (longitudinal) and T (transverse). The longitudinal and transverse curves correspond to polarizations of the electrical field along and across the strike of the prism respectively. The ρ_A(3-D) curves are compared with the ρ_A(2-D) curves generated by the TM and TE modes in a 2-D model containing the prism, with $l \to \infty$. The 1-D curve ρ_A(1-D) is shown too. This curve corresponds to the 1-D model that is reached at $l \to \infty$ and $w \to \infty$. It stands for a normal curve.

The ρ_A(3-D) curves differ drastically from the normal ρ_A(1-D) curve. These distortions result from the current-gathering effect. However, note that the transverse ρ_A(3-D, T) curve is close to the ρ_A(2-D, TM) curve, so its 2-D inversion can yield a trustworthy geoelectrical profile. At the same time the longitudinal ρ_A(3-D, L) curve shows a striking departure from the ρ_A(2-D, TE) curve, so its 2-D inversion will introduce a spurious conductor.

It is evident that in the model with the conductive prism the TM impedance is more robust to 3-D effects than the TE impedance is. But can we expand this remarkable property of the TM mode to the general case?

Let us return to model C and replace the prism of $2\ \Omega$ m resistivity by a prism of the same geometry but of $40\,000\ \Omega$ m resistivity ($\rho_P \gg \rho_S$). Now we simulate a mountain root rather than a valley, and observe currents flowing around instead of currents gathering. The curves of ρ_A(3-D), ρ_A(2-D) and ρ_A(1-D) are displayed on the right-hand side of Fig. 6. We see that the relationship between the 3-D and 2-D curves changes radically. In fact, in the model with a resistive prism, both of the 3-D curves are close to their 2-D counterparts. What is more, the longitudinal ρ_A(3-D, L) curve is close not only to the ρ_A(2-D, TE) curve but even to the normal curve ρ_A(1-D). The longitudinal 3-D response corresponding to the TE mode is almost undistorted! It admits not only 2-D inversion, but even 1-D inversion.

In model C, with the resistive prism, the around-flow effect consists of three elements: over-flow (currents flow over the prism), under-flow (currents flow under the prism) and side-flows (currents flow at the sides of the prism). Here the over- and under-flow effects prevail, and this is why the ρ_A(3-D, T) curve is close to the ρ_A(2-D, TM) curve.

Let us construct model D, where the resistive prism is transformed into a 3-D horst-like elevation approaching the

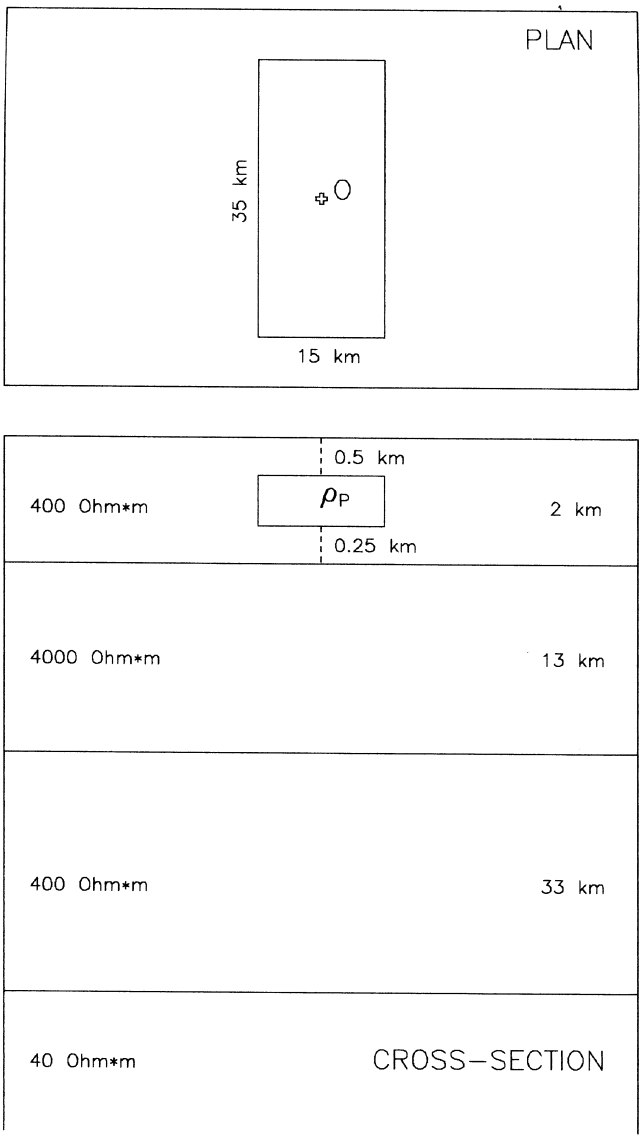

Figure 5. Model C: a 3-D elongated prism of resistivity ρ_P in the first layer (not to scale). O, sounding site.

Earth's surface (Fig. 7). Here the length and width of the elevation are $l = 12$ km and $w = 2$ km, its elongation being $e = l/w = 6$. One can expect that in this model the side-flow effect will dominate, and the agreement between the ρ_A(3-D, T) and ρ_A(2-D, TM) curves will be violated. Fig. 8 shows the 3-D transverse and longitudinal curves ρ_A(3-D, T) and ρ_A(3-D, L) obtained along the central profile at different distances from the elevation edge (5, 3 and 1 km, sites A, B and C respectively). Also shown are the 2-D curves ρ_A(2-D, TM) and ρ_A(2-D, TE) corresponding to a model with an infinitely long elevation, and the 1-D ('normal') curves ρ_A(1-D) for a model without an elevation. It is notable that at all sites the longitudinal curves ρ_A(3-D, L) practically coincide with the ρ_A(2-D, TE) and ρ_A(1-D) curves. Clearly, they allow for 2-D and even 1-D inversion. At the same time the transverse curves ρ_A(3-D, T) go below the ρ_A(2-D, TM) curves, and this depression drastically increases in the immediate vicinity of the prism. At site C (1 km from the elevation edge) the ρ_A(3-D, T) curve tips over, and the degree of its distortion is almost the same as in the case of the longitudinal ρ_A(3-D, L) curve in model C with a conductive prism. Going to the impedance phases, we note that depression of the ρ_A(3-D, T) curves is accompanied by severe deformation of the φ(3-D, T) curves. These properties of the around-flow effect indicate its galvanic–inductive nature (the intensity of a current around-flow is governed by the horizontal skin effect in the conductive medium surrounding a resistive body). Clearly, the formal 2-D inversion of the transverse curves will introduce a spurious conductor.

Thus, the accuracy of 2-D approximation of 3-D structures depends on their conductivity. According to Berdichevsky *et al.* (1995) an elongation of a body $e \geq 3$–5 ensures 2-D approximation with 10 per cent accuracy in the apparent resistivities if a conductive body is in the TM field or if a resistive body is in the TE field. This simple criterion is valid for both shallow and buried structures. Analysis of models C and D adds considerable support to these estimates.

It seems that the wording 'The TM impedance is more robust to plausible 3-D effects than the TE impedance' (Wannamaker *et al.* 1989) should be changed. The best answer to the question about the robustness of the TM and TE modes may be the following: 'The TM impedance is more robust to 3-D effects caused by conductive structures (that is, by current gathering), but the TE impedance may be more robust to 3-D effects caused by resistive structures (that is, by current around-flow)'.

STATIC EFFECTS IN THE TM AND TE MODES

Static effects are caused by inhomogeneities in the upper layers of the Earth. They manifest themselves in a vertical shift of apparent resistivity curves in the period range $T > T_S$, whereas the shapes of the shifted curves and the corresponding section of the phase curves remain unchanged (Berdichevsky & Dmitriev 1976a; Jones 1988; Vozoff 1991; Weaver 1994; Zhdanov & Keller 1994). At these periods, the skin depth is much larger than the thickness of the inhomogeneity, so that the local induction dies out and the anomalous field becomes quasi-static (galvanic). Clearly, the initial period T_S bounding the period range of static shift depends on the dimensions and position of the causative inhomogeneity.

For the sake of definiteness, we have to specify a reference line for the static shift. It would be natural to reckon the static shift from the normal 1-D or 2-D curves calculated for the observation site. Unfortunately such estimations are possible only in theory. In practice, we detect and evaluate the static shift using adjacent or averaged MT curves.

Fig. 9 shows some 2-D models with different inhomogeneities in the first layer (the sedimentary cover). As in many previous models in this paper, we consider the 2-D curves ρ_A(2-D, TM), ρ_A(2-D, TE) and φ(2-D, TM), φ(2-D, TE) at the central site O and the 1-D ('normal') curves ρ_A(1-D, O), ρ_A(1-D, R) and φ(1-D, O), φ(1-D, R) at the central site O and the remote site R (Fig. 10). The remote curves ρ_A(1-D, R) and φ(1-D, R) can be considered as a background.

Model E simulates a local near-surface inhomogeneity. Here a small resistive body contacts the Earth's surface. Take a look at the apparent resistivity and impedance phase curves. Within the period range $T > T_S$, where $T_S = 0.1$ s, the transverse curve ρ_A(2-D, TM), consisting of ascending and descending branches, faithfully copies the normal curves ρ_A(1-D, O) and ρ_A(1-D, R) but is shifted upwards by a constant factor which depends on

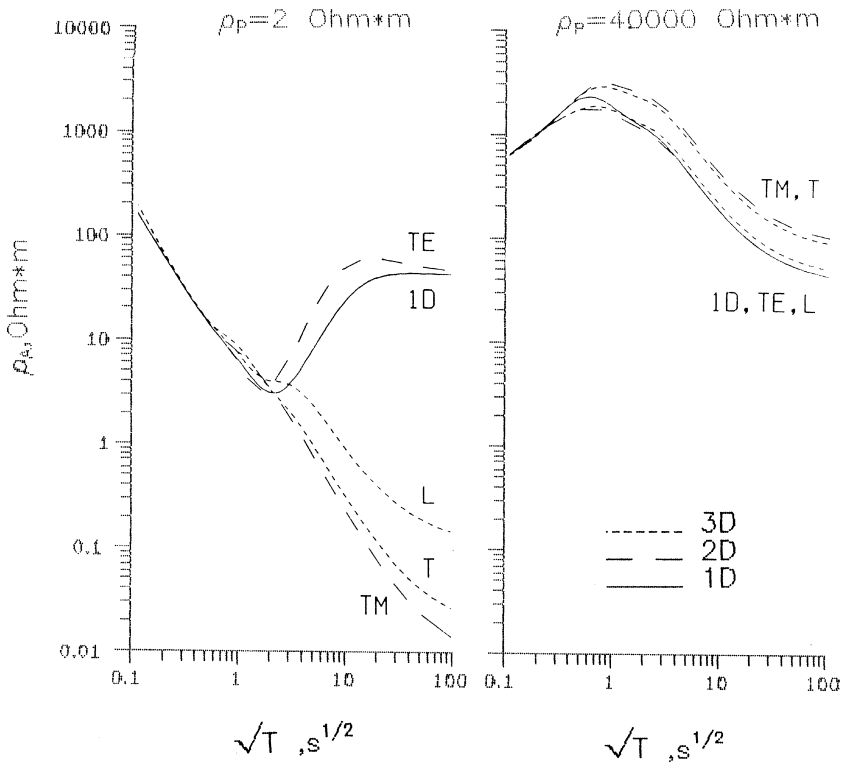

Figure 6. Apparent resistivity curves in model C for MT sounding at site O; ρ_P, prism resistivity. Solid lines: 1-D curves. Dashed lines: long dashes, 2-D curves for TE and TM modes; short dashes, 3-D curves for longitudinal (L) and transverse (T) polarizations of the electric field.

the geometry of the inlier and its resistivity. At periods $T < T_S$, a difference appears between the ρ_A(2-D, TM) curve and the ρ_A(1-D, O) and ρ_A(1-D, R) curves. The static shift of this type is called a ρ effect. The ρ effect does not affect the transverse curve φ(2-D, TM) or the longitudinal curves ρ_A(2-D, TE), φ(2-D, TE), which, in the same period range, merge with the normal curves ρ_A(1-D, O), φ(1-D, O).

Models F and G simulate a horst-like elevation of resistive rocks and variations in resistivity of the sediment series. They demonstrate somewhat different relations. It is immediately apparent that the ascending branch of the transverse ρ_A(2-D, TM) curves is not distorted, as it merges with the normal curves of ρ_A(1-D, O). Here the static shift begins at $T_S \approx 100$ s. It does not affect the ascending branch of the ρ_A(2-D, TM) curves, but it displaces the descending branch upwards by the constant factor $\log(S_h/S_i)$, where S_h and S_i are the sediment conductances in the host and inhomogeneity areas. The static shift of this type is called an S effect. Note that in the same period range the descending branch of the longitudinal ρ_A(2-D, TE) curve merges with the normal curve ρ_A(1-D, O), and the phase curves φ(2-D, TM), φ(2-D, TE) approach their normal counterparts φ(1-D, O), φ(1-D, R).

Behind the ρ and S effects are the same physical mechanisms; however, they operate in different frequency intervals. When correcting the ρ effect (model E), we have to displace both the ascending and the descending branches of the ρ_A curves. In the case of the S effect (models F and G), only the descending branch should be displaced.

How can we recognize the ρ and S effects in data? In all three models the relations between the apparent resistivity curves are almost the same: the ρ_A(2-D, TM) and the remote ρ_A(1-D, R) curves are identical in shape (including their ascending and descending branches). Considering the ρ_A curves, we cannot tell the ρ effect from the S effect. The phase curves are more informative, since they help to mark the bounding period T_S: in model E the curves φ(2-D, TM) and φ(1-D, R) merge at the very beginning of the ascending branch of the ρ_A(2-D, TM) curve (the ρ effect), but in models F and G they merge close to the maxima of the ρ_A(2-D, TM) curves (the S effect). So, the period T_S can be defined as the period at which adjacent phase curves merge together.

These relations allow us to suggest a simple rule for static shift corrections. The ρ_A curves should be corrected at periods with coincident phases.

Other evidence can be obtained by correlating the apparent resistivities ρ_A with the sediment conductance S determined from frequency or transient soundings. If, for instance, the ρ_A values of the ascending branches of the apparent resistivity curves do not correlate with the S values, then they are distorted by the ρ effect. Conversely, if the ρ_A values of the low-frequency descending branches of the apparent resistivity curves do correlate with the S values, then they are distorted by the S effect.

2-D modelling gives the simplest examples of static shift, with only the TM mode suffering from the ρ and S effects. In actual practice, we deal with a superposition of elongated structures and local 3-D inhomogeneities. So, both of the E field polarizations are distorted, and hence not only the transverse but also the longitudinal apparent resistivity curves suffer to some extent from the ρ and S effects.

Though the static shift changes neither the shape of the long-period part of the ρ_A curves nor the corresponding phases, it severely plagues the interpretation of MT data. The success of 2-D MT interpretation depends greatly on the reliability of

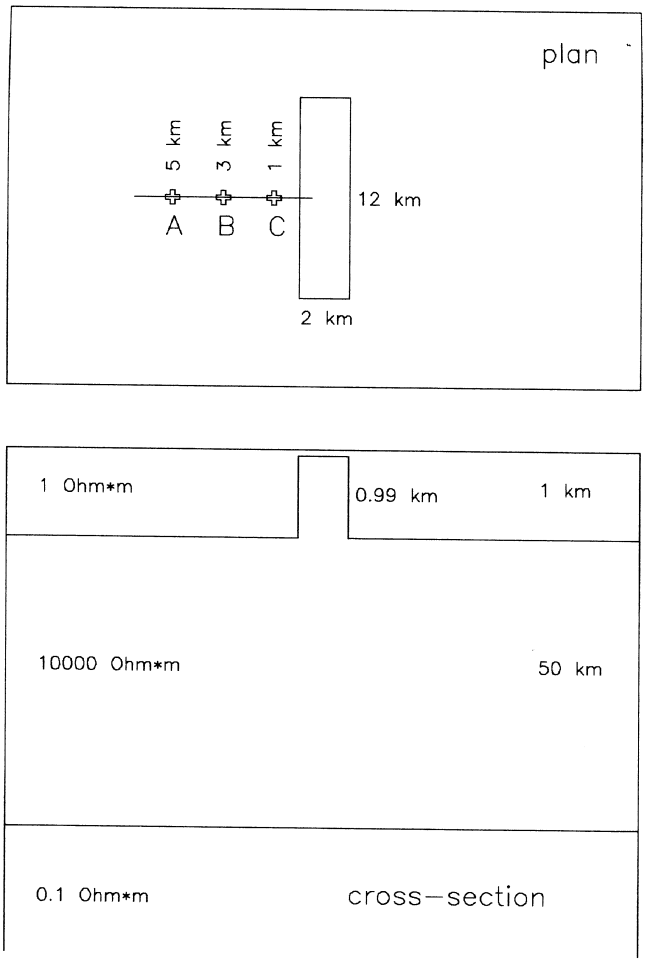

Figure 7. Model D: a 3-D horst-like resistive elevation in the sedimentary cover (not to scale); A, B, C, sounding sites with their distances to the edge of the elevation.

the static-shift corrections. We would like to stress that there is no standard universal remedy for static shift; the best result can be attained by combining different correction techniques and controlling them by phase inversion and independent geological or geophysical data.

When inserting real MT data into the 2-D interpretation model, we have to suppress the noise caused by the ρ effect in the transverse and longitudinal ρ_A curves, and correct the longitudinal ρ_A curves distorted by the S effect.

Modern magnetotellurics offers a number of methods for the static-shift correction (Bostick 1986; Jones 1988; Berdichevsky, Vanyan & Dmitriev 1989; Pellerin & Hohmann 1990; Vozoff 1991; Zinger 1992). These methods reduce to statistical averaging, filtering, displacement to some reference values and mathematical modelling.

Non-interpretable noise caused by the ρ effect can be successfully suppressed by the EMAP technique (Bostick 1986; Torres-Verdin & Bostick 1992), by statistical averaging and filtering of the apparent resistivities (Berdichevsky *et al.* 1980) or by smoothing high-frequency inversions of apparent resistivities (Ingham 1996). In regions where homogeneous sediments contain small near-surface inliers, the displacement of the ρ_A curves to the host resistivity determined by means of transient soundings is rather efficient (Sternberg, Washburne & Pellerin 1988; Kaufman 1988; Pellerin & Hohmann 1990). For the study of sedimentary basins, a method based on the parametrization of slow lateral variations in the resistivity of deep layers may be of use (Jones 1988).

The most simple technique for correcting the S effect is displacement of the low-frequency branches of the ρ_A curves ($T = 2$–5 hr) to the standard ρ_A curve, produced from global geomagnetic sounding and large magnetotelluric statistics (Rokityansky 1982; Fainberg 1983; Berdichevsky *et al.* 1989). Unfortunately, this attractive method can only be applied with some limitation, say, in the stable geological provinces (or at least away from anomalous zones such as rifts, subductions and plumes), where the mantle conductivity at depths of about 300–500 km rarely experiences gross changes in the horizontal directions. However, we can extend the capabilities of the method by using some regional (or even local) magnetovariation references related to different geological provinces (Semenov *et al.* 1993; Trapeznikov *et al.* 1997). Some procedures based on averaging and filtering of ρ_A curves may be helpful also (Dmitriev & Berdichevsky 1988; Berdichevsky *et al.* 1988). Among recent developments, the method of dynamic correction is particularly promising (Fainberg *et al.* 1995). The basic idea of the method is rather simple. Given the S distribution, a thin-sheet model of inhomogeneous sedimentary cover can be constructed which allows for determining the distortion matrix.

In any case, the inversion of shift-corrected ρ_A curves should be supported and controlled by the inversion of φ curves. Note that such a control is reasonable if the apparent resistivities and phases satisfy the dispersion (minimum-phase) relation (Fischer & Schnegg 1993; Berdichevsky & Pokhotelov 1996).

THE TM MODE IN THE PRESENCE OF DEEP FAULTS

Deep faults bearing fluids or graphite form conductive channels that cross the high-ohmic lithosphere and cause redistribution of telluric currents induced in different layers of the Earth's crust and upper mantle. Under the influence of conductive faults, the magnetotelluric field takes on quite new properties (Dmitriev *et al.* 1982; Kovtun & Vardanyants 1985; Park *et al.* 1991; Berdichevsky, Dmitriev & Kulikov 1993; Berdichevsky & Kulikov 1994; Berdichevsky, Dmitriev & Kulikov 1994). Let us consider two models illustrating the effect of conductive faults.

Fig. 11 presents the 2-D model H, with a resistive inclusion (the horst) in the first layer (the sedimentary cover) and narrow vertical channels of resistivity ρ_F in the second layer (the high-ohmic crust). The lower part of the model consists of the crustal conductive layer, the resistive mantle and the conductive asthenosphere. The type of model depends on the choice of ρ_F.

If $\rho_F = 100\,000\ \Omega$ m, the model lacks vertical conductive channels, and the curve ρ_A(2-D, TM) obtained at the central site O suffers severely from the S effect. It is shaped like the remote normal curve ρ_A(1-D, R), being shifted upwards by two decades, while the curves φ(2-D, TM) and φ(1-D, R) merge close to the maximum of the ρ_A(2-D, TM) curve.

Now let $\rho_F = 10\ \Omega$ m. In this model the horst is fringed by conductive channels (fluidized or graphitized faults) which connect the sediments with the crustal conductive layer. Thus, we have a closed conductive circuit which shunts the horst (a bypass for excess currents). Here the ρ_A(2-D, TM)

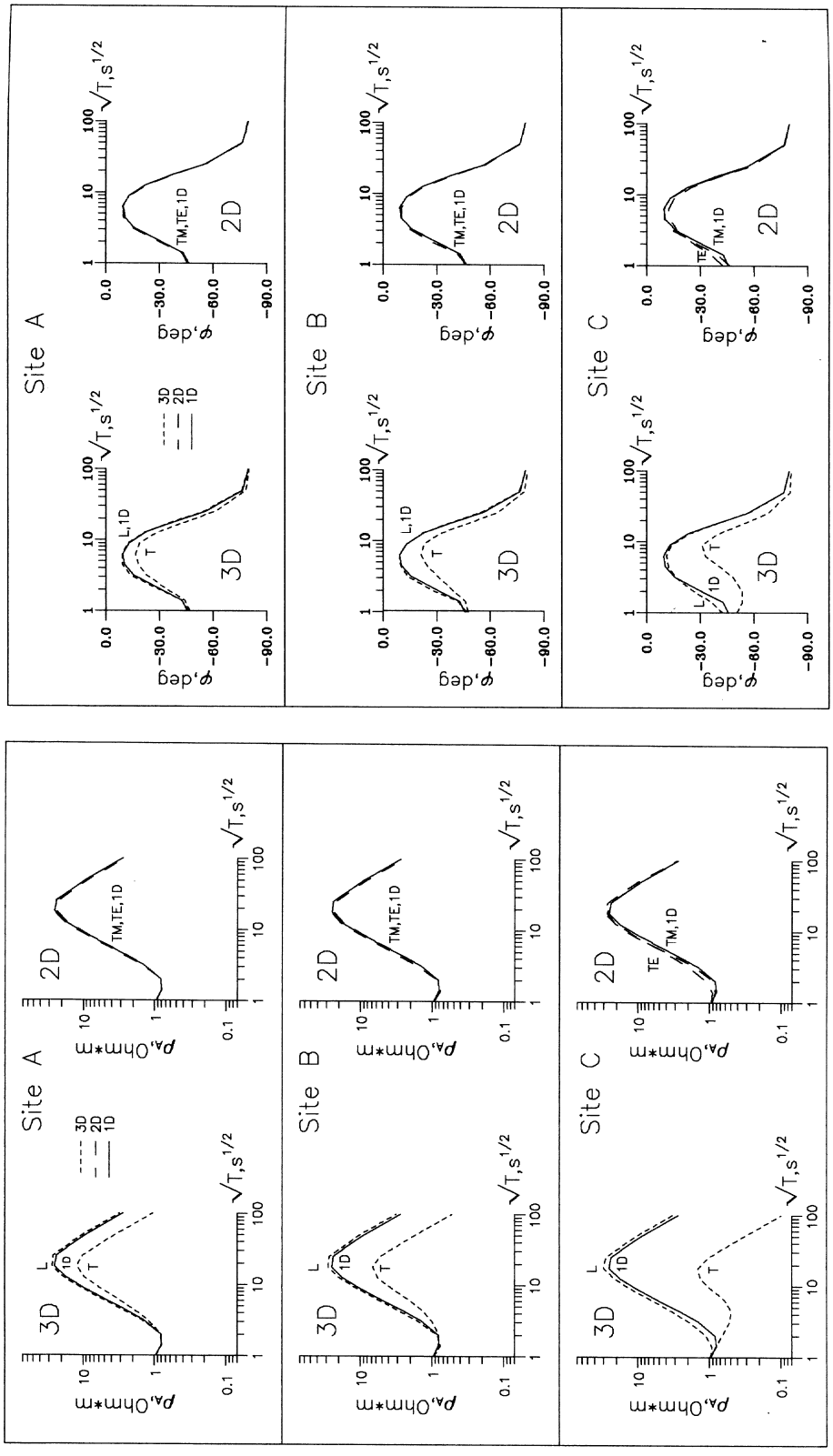

Figure 8. Apparent resistivity and phase curves in model D. MT soundings at sites A, B, C. Solid lines: 1-D curves. Dashed lines: long dashes, 2-D curves for TE and TM modes; short dashes, 3-D curves for longitudinal (L) and transverse (T) polarizations of the electric field.

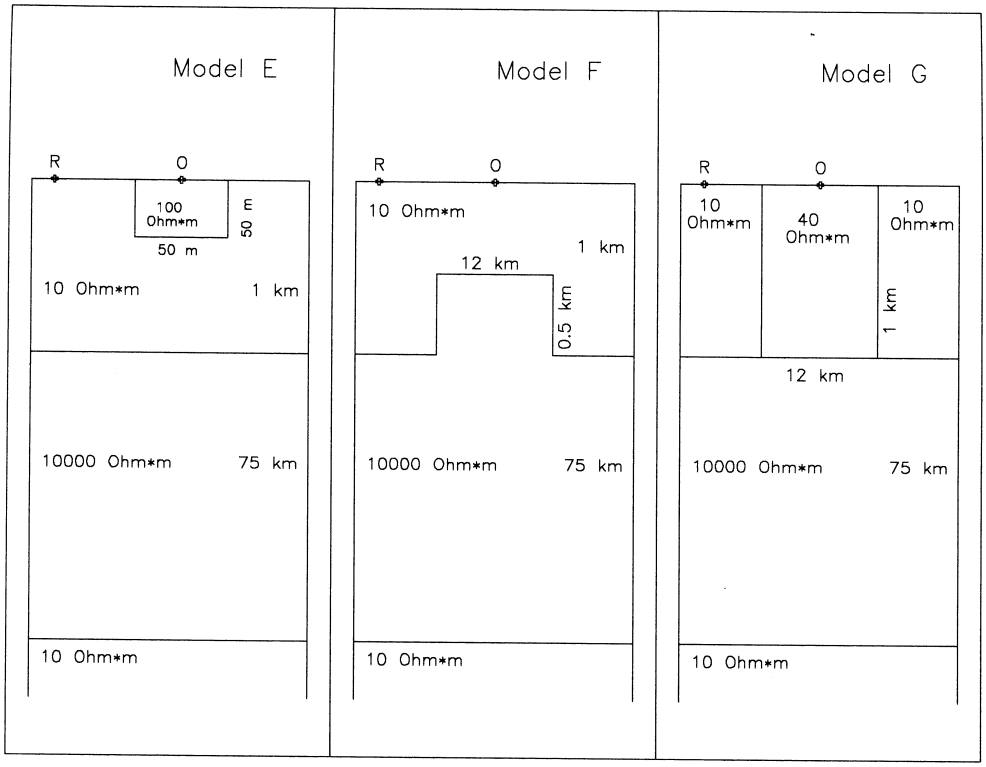

Figure 9. Different inhomogeneities in the sedimentary cover. Model E: a local near-surface resistive inhomogeneity; model F: a horst-like elevation of resistive rocks; model G: an increase of sediment series resistivity. O, R, sounding sites.

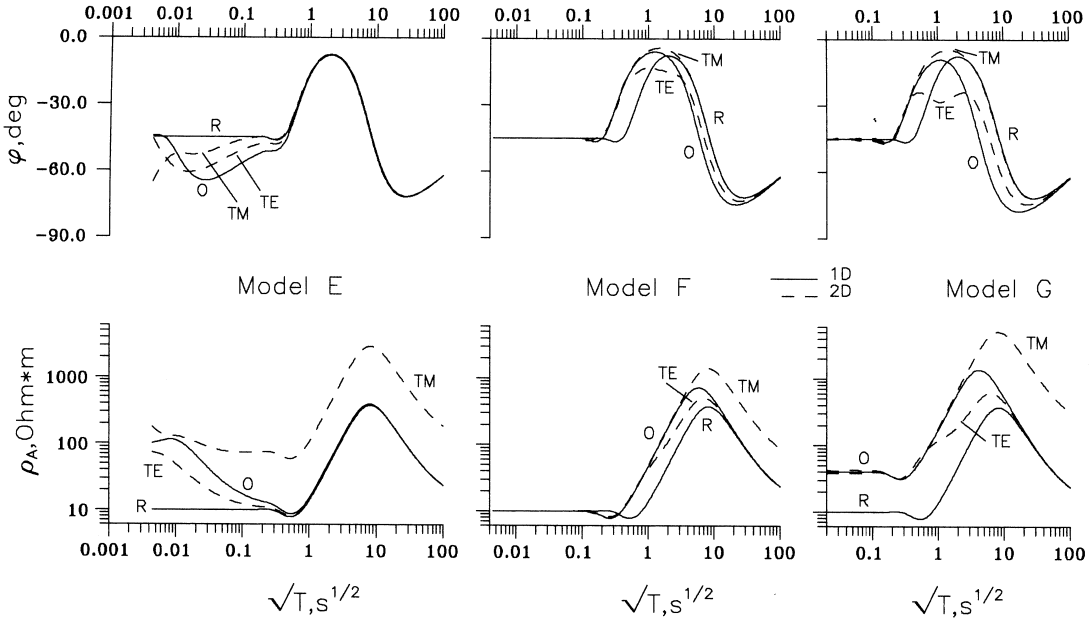

Figure 10. Apparent resistivity and impedance phase curves in models E, F and G. Model E shows the ρ effect, models F and G show the S effect. Solid lines: 1-D curves at central site O and remote site R; dashed lines: 2-D curves for the TE and TM modes at central site O.

and φ(2-D, TM) curves obtained at the central site O are almost undistorted, being close to the central normal curves ρ_A(1-D, O) and φ(1-D, O). It seems that conductive faults may kill the S effect in the TM mode.

Fig. 12 shows the 2-D model I, with an asthenosphere elevation bordered by vertical channels of resistivity ρ_F. If $\rho_F = 100\,000\ \Omega$ m, we return to model B (Figs 3 and 4), where the TM mode is insensitive to the relief of the asthenosphere (the screening effect). Here the ρ_A(2-D, TM) and φ(2-D, TM) curves obtained at the central site O merge with the remote normal curves ρ_A(1-D, R) and φ(1-D, R). Now let $\rho_F = 10\ \Omega$ m. Here the asthenosphere elevation is connected with the sediments, and the ρ_A(2-D, TM) and φ(2-D, TM) curves virtually merge with the central normal curves ρ_A(1-D, O) and

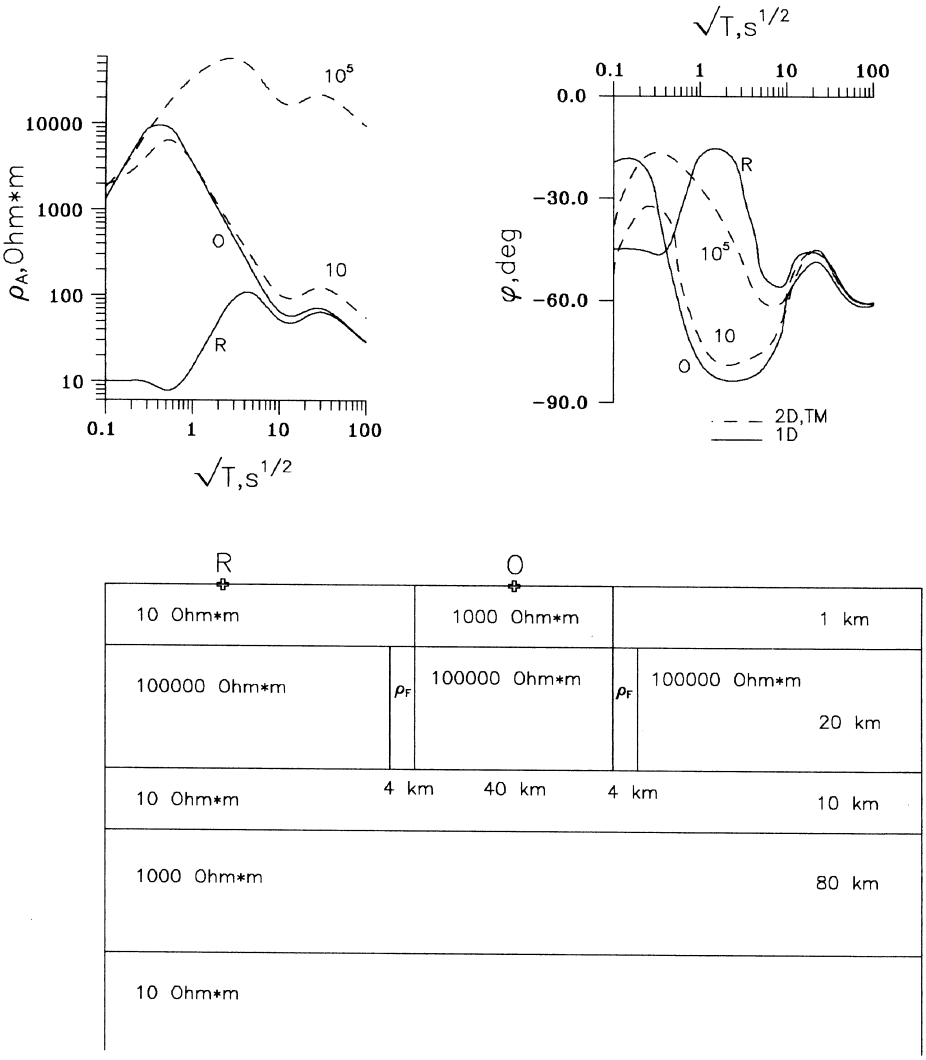

Figure 11. Model H: a resistive inclusion in the sedimentary cover and vertical channels in the high-ohmic crust. Top: apparent resistivity and impedance phase curves. Solid lines: 1-D curves at central site O and remote site R; dashed lines: 2-D curves for the TE and TM modes at central site O, numbered with the channel resistivity. Bottom: cross-section of the model (not to scale); ρ_F, channel resistivity; O, R, sounding sites.

φ(1-D, O), reflecting the relief of the asthenosphere. It seems that conductive faults may kill the screening effect in the TM mode.

Concluding the analysis of these models, we note that the TM mode may have a rather high sensitivity to conductive faults which connect near-surface and deep conductors and form closed current circuits.

SOME PRACTICAL EXAMPLES

It is useful to supplement the results of the analysis of the above models with some examples from Russian magnetotelluric practice. These examples show that under favourable conditions (elongated resistive structures in sediments without local 3-D inliers) the longitudinal curves of apparent resistivity may suffer less from the static shift.

At the top of Fig. 13 we see longitudinal (L) and transverse (T) apparent resistivity curves which have been obtained in the vicinity of the Urals (Dyakonova, Ingerov & Rokityansky 1986). It is obvious that here the longitudinal ρ_A curves experience a far lesser static shift than the transverse ρ_A curves do. The descending, mantle branches of the longitudinal curves are close to each other. They gravitate to the standard curve of ρ_{st}. At the same time the corresponding transverse curves cross the ρ_{st} curve and their mantle branches are shifted upwards by one-half of a decade or even more.

At the bottom of Fig. 13 we see longitudinal and transverse ρ_A curves obtained in the Kola Peninsula (Dyakonova *et al.* 1986). Here almost the same pattern is observed. The longitudinal curves are slightly distorted. Their left-hand descending branches merge together, reflecting a conductive layer in the lower part of the Earth's crust. The mantle branches of these curves are arranged about the standard curve of ρ_{st}, though with a slightly different slope. Compare the longitudinal curves with the transverse ones. The transverse curves cross the ρ_{st} curve, being drastically shifted upwards (by up to two decades).

A large number of researchers (Kovtun 1989; Moroz 1991; Dyakonova *et al.* 1986; Alperovich *et al.* 1980) testify that above relations between longitudinal and transverse MT curves are observed in many regions of Russia. It is quite clear to us that if longitudinal MT curves are less distorted by static shift, they have some advantages for interpretation.

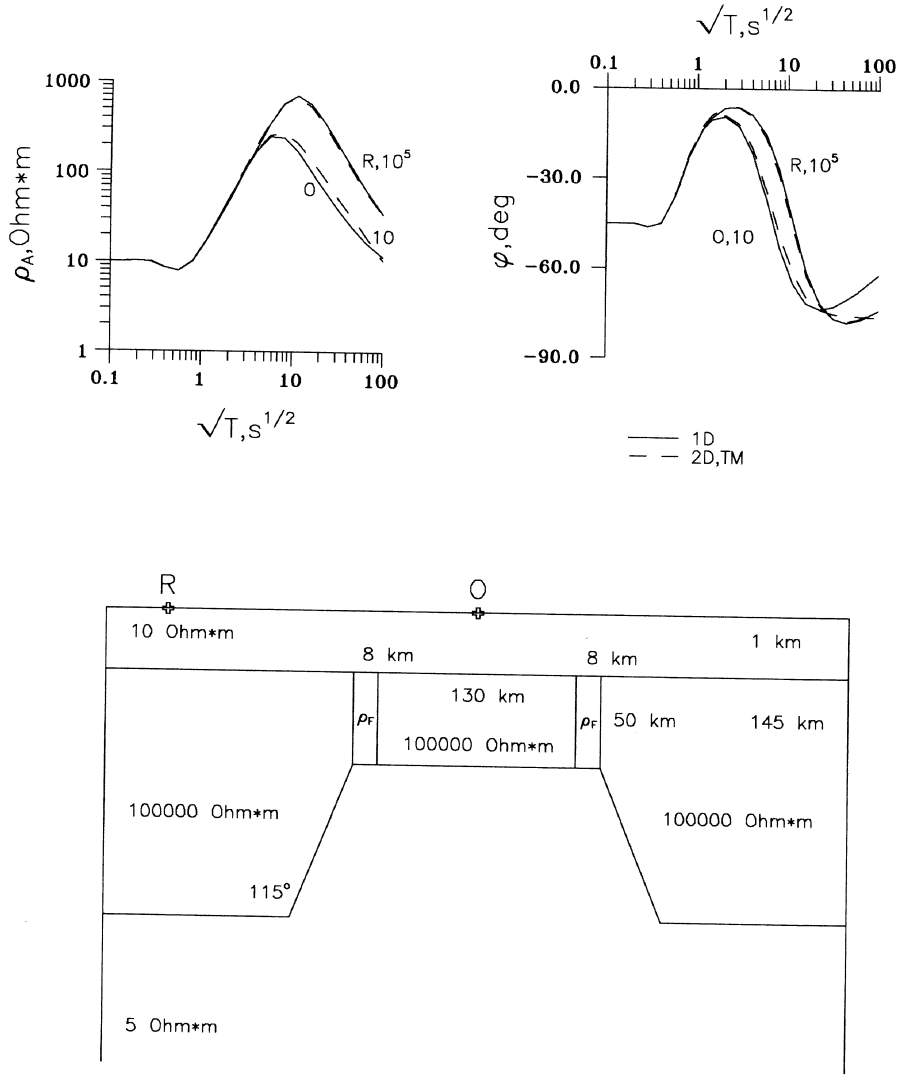

Figure 12. Model I: an asthenosphere elevation bordered by vertical channels crossing the high-ohmic lithosphere. Top: apparent resistivity and impedance phase curves. Solid lines: 1-D curves at central site O and remote site R; dashed lines: 2-D curves for the TE and TM modes at central site O, numbered with the channel resistivity. Bottom: cross-section of the model (not to scale); ρ_F, channel resistivity; O, R, sounding sites.

The last example appears worthy of more extended discussion. It shows that in some regions the longitudinal apparent resistivity curves may play a leading role. Fig. 14 presents the longitudinal ($\rho^{\parallel}$) and transverse ($\rho^{\perp}$) apparent resistivity curves observed along a profile crossing the Precaucasian foredeep (Berdichevsky & Dmitriev 1976b). The longitudinal $\rho^{\parallel}$ curves are bowl-type throughout the entire profile, 150 km long. Their 1-D interpretation gives a Palaeozoic basement relief that is in close agreement with seismic measurements and drillings. At the same time the transverse $\rho^{\perp}$ curves change their shape, from bowl-type at a distance of 120–150 km from mountains to a descending type in the vicinity of mountains. It is small wonder that 1-D and even 2-D interpretations of the transverse $\rho^{\perp}$ curves give incongruous results that have nothing in common with seismic data or general geological ideas of the structure of the region. Suffice it to say that with TM inversion the resistivity of the sediments falls to 0.1 Ω m, while the solid high-ohmic lithosphere wedges out and the conductive 'asthenosphere' appears at a depth of about 8–10 km. It seems that this remarkable situation is the same as in model D, where transverse currents flow around a 3-D resistive elevation (Figs 7 and 8). The resemblance in behaviour of the experimental and model MT curves is striking. It can be assumed that within the Precaucasian foredeep we observe an intense 3-D effect connected with currents flowing around the high-ohmic Caucasian Ridge. The flow-around effect dramatically distorts the transverse $\rho^{\perp}$ curves (the TM mode) and scarcely affects the longitudinal $\rho^{\parallel}$ curves (the TE mode). Some of our colleagues adhere to TM inversion because '2-D interpretation of the TM mode is more accurate than the TE mode in the presence of 3-D bodies' (Park 1996). We would be very grateful if they showed us how to interpret the transverse ρ_A curves obtained in the vicinity of the Caucasian Ridge.

THE PRINCIPLE OF COMPLEMENTARITY IN MAGNETOTELLURICS

We have examined the main properties of transverse and longitudinal MT curves observed in the vicinity of elongated structures. The results of this examination are summarized in Table 1.

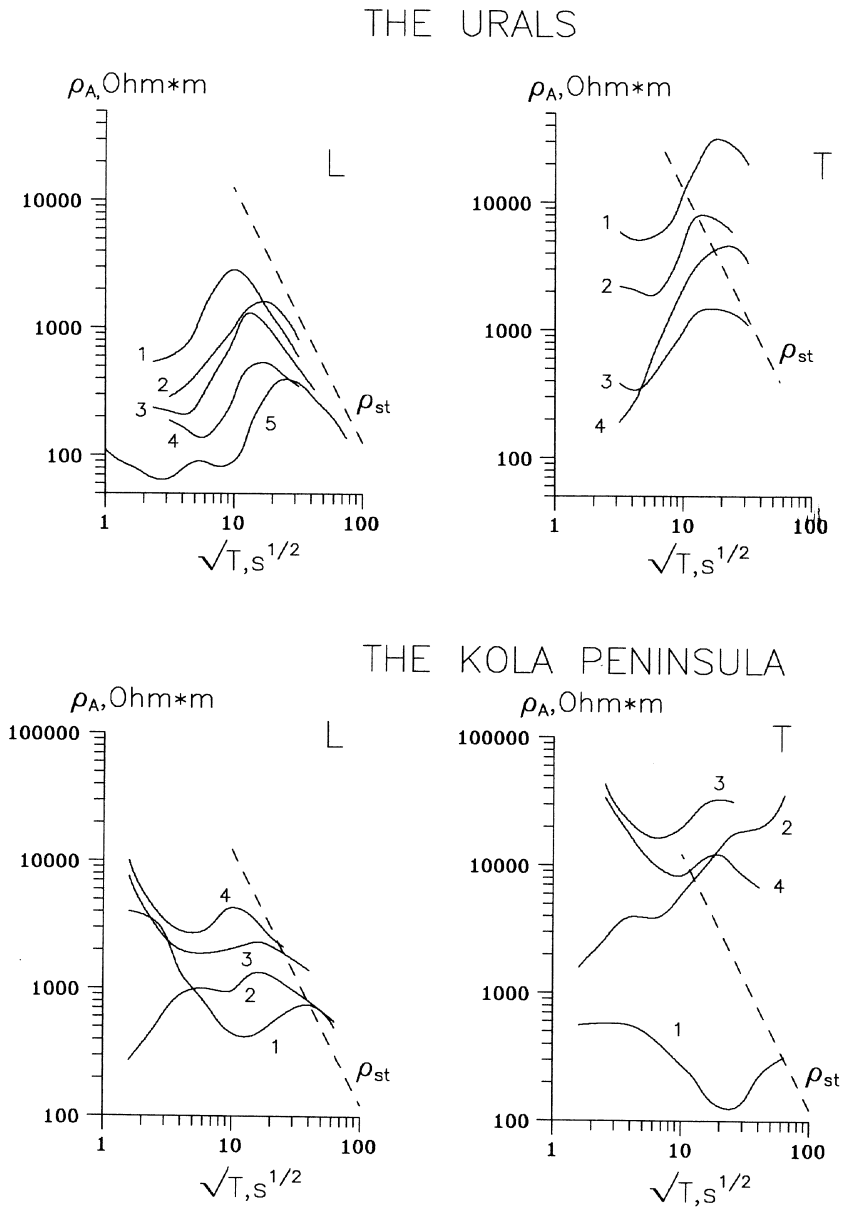

Figure 13. Longitudinal (L) and transverse (T) apparent resistivity curves characteristic of the Urals (top) and the Kola Peninsula (bottom); ρ_{st}, standard apparent resistivity curve; the numbers 1–5 indicate the MT sounding sites.

Table 1. Properties of transverse and longitudinal MT curves, ⟨…⟩, favourable property.

MT CURVES		TRANSVERSE	LONGITUDINAL
Accuracy of 2D approximation of:	conductive structure	⟨higher⟩	lower
	resistive structure	may be lower	⟨may be higher⟩
Sensitivity to:	near-surface structure	⟨higher⟩	lower
	deep structure	lower	⟨higher⟩
	lithosphere resistance	⟨higher⟩	lower
	deep fault	⟨may be higher⟩	may be lower
Static shift		larger	⟨smaller⟩

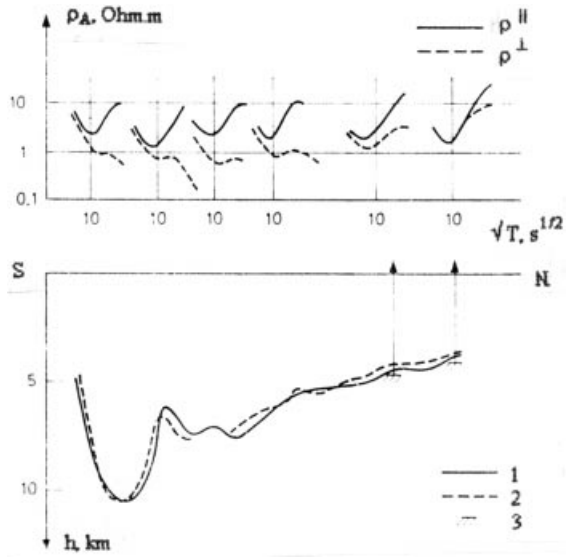

Figure 14. Top: longitudinal ($\rho^{\parallel}$) and transverse ($\rho^{\perp}$) apparent resistivity curves along a profile crossing the Precaucasian foredeep. Bottom: geophysical cross-section: surface of the Palaeozoic basement from (1) the $\rho^{\parallel}$ curves, (2) seismics, (3) drilling.

While the transverse MT curves provide higher accuracy in the 2-D approximation of conductive structures and higher sensitivity to near-surface structures and to the lithosphere resistance and deep faults, the longitudinal MT curves provide higher sensitivity to deep structures and may ensure higher accuracy in the 2-D approximation of resistive structures. If the transverse curves suffer dramatically from the static shift, the longitudinal curves may be almost undistorted. The transverse and longitudinal MT curves nicely complement each other: gaps left by one mode are filled by another mode. In this sense we say that the TM and TE modes satisfy the principle of information complementarity. The complementarity principle forms a sound basis for the 2-D interpretation strategy.

The sensitivity to the structures that are the targets of the MT soundings is of critical importance. Say, for instance, that conductive zones in deep layers of the high-ohmic lithosphere are to be studied, and the sensitivity of the TM mode is too poor for this task (no deep conductive faults, severe galvanic screening). In this case, the TE mode with its higher sensitivity to buried conductors is the only contributor of useful information. The situation is paradoxical. We have to abandon the TM mode with its high accuracy of 2-D approximation, and harness the less accurate TE mode. There is no way to the necessary information except by using the TE mode with all its problems.

If we were asked 'Is it not better to ignore the TE mode, with its potentiality of erroneous conductors, and to start with the TM mode, which does not yield any conductors but closely fits the data?', we would answer 'It is better to get rough (maybe even qualitative) information than no information'. Our philosophy accords with Vozoff's statement (Vozoff 1991) that 'exploration problems sometimes require a simple "yes" or "no" answer to the questions such as "does a buried conductor exist here?"'. Thus, we use TE inversion and try to control its errors by means of 3-D estimates.

In closing, we state that in the general case the most comprehensive and reliable information on the Earth's conductivity can be derived by means of bimodal inversion, that is using both the TM and the TE mode (the transverse and longitudinal MT curves).

GENERAL SCHEME OF 2-D MT INTERPRETATION

Geophysicists know a lot of different methods and techniques for 2-D interpretation of MT soundings. All of these approaches fall into a simple scheme consisting of three stages.

(1) Construction of an interpretation model (a compact set of all acceptable solutions). At this stage, uniting *a priori* geological–geophysical information with the results of qualitative analysis of observation data (impedance tensors, tippers and apparent resistivities), we have to detect 3-D distortion effects which cause spurious structures in TM and TE inversion (current gathering or flowing around), eliminate artefacts, design the geoelectrical background, estimate the degree of horizontal inhomogeneity of the medium, outline different geoelectrical zones and establish their dimensionality, trace deep conductive faults and examine their effects, separate regional (2-D) and local (2-D and 3-D) effects, identify elongated structures and define their strike, evaluate the screening effect, choose the limiting values of the electromagnetic parameters, fix the 2-D interpretation model and suggest the strategy for bimodal inversion. *A priori* 3-D modelling of known structures in order to estimate the accuracy of 2-D approximations to them is very useful at this stage of MT interpretation.

(2) Formal, regularized inversion of observation data. The inversion is carried out on the compact set of all acceptable 2-D solutions. It reduces to static shift corrections, choice of a starting model and minimization of the misfit between theoretical and experimental characteristics. This stage of interpretation terminates in constructing a geoelectrical model that is in good agreement with *a priori* information and the observation data. Different approaches can be applied (deterministic, stochastic, non-linear or linearized). The choice of one or another of the approaches is a question of technology, since all of them are almost equivalent with respect to the resulting information.

(3) Geological, hydrological, petrophysical and geodynamic analysis of the geoelectrical model (stratigraphic identification of rocks; determination of their texture, porosity, penetrability and saturation by fluids; prognosis of deposits; geodynamic estimates; etc.). At this concluding stage we return to the *a priori* information and involve the results of laboratory measurements and well-logging, seismic data and data from other geophysical methods.

TWO-LEVEL ALGORITHM FOR THE BIMODAL INVERSION

The algorithm for bimodal inversion should be selective. It must emphasize the most reliable and suppress the least reliable elements of the model derived from the different field modes. While estimating the reliability of different geoelectrical elements, we have to proceed primarily from the sensitivities of the TM and TE modes. For example, if a lithosphere conductor is strongly screened in the TM mode but shows up vividly in the TE mode, preference must be given to the TE mode, though

the accuracy of the 2-D approximation of conductors in the TE field is much lower than in the TM field.

The selectivity of the bimodal algorithm can be attained by separating the TM and TE inversions and using weighted functionals (Berdichevsky *et al.* 1992; Golubev & Varentsov 1994; Berdichevsky *et al.* 1995). This philosophy is realized in an algorithm which includes two levels (Fig. 15). We shall consider a bimodal two-level algorithm, as applied to deep MT soundings in regions with a severe screening effect of the high-ohmic lithosphere.

Level 1 (the TE inversion)

At this level, inversion of the TE mode is accomplished using the longitudinal ρ_A and φ curves. The main objective of the TE inversion is to optimize deep conductive zones in the consolidated crust and upper mantle. The inversion is stabilized by proximity to the starting model $\sigma_0(x, z)$, which has been constructed on the basis of *a priori* information and qualitative or even quantitative analysis of observation data (including a rough interpretation of magnetovariation anomalies). It reduces to iterative minimization of the Tikhonov functional, consisting of apparent resistivity and phase misfits and a model stabilizer (Tikhonov & Arsenin 1977),

$$\Phi^{TE} = \int_x \int_T w_1(x, T) \left| \ln \frac{\rho_A(3\text{-D, L})}{\rho_A(2\text{-D, TE})} \right|^2 \frac{dT}{T} dx + \int_x \int_T w_2(x, T) |\varphi(3\text{-D, L}) - \varphi(2\text{-D, TE})|^2 \frac{dT}{T} dx + \alpha \int_x \int_z w_3(x, z) |\sigma(x, z) - \sigma_0(x, z)|^2 dz dx, \quad (1)$$

where T is the period of variation, x is the coordinate of the observation site, ρ_A(3-D, L) is the observed value of longitudinal apparent resistivity corrected for ρ and S effects, φ(3-D, L) is the observed value of longitudinal impedance phase, ρ_A(2-D, TE) and φ(2-D, TE) are the theoretical values of apparent resistivity and phase for the 2-D model $\sigma(x, z)$ excited by an E-polarized field, w_1 and w_2 are weights representing the reliability and informativeness of different sections of the MT curves, w_3 is a weight expressing the degree of confidence in the different elements of the starting model $\sigma_0(x, z)$, and α is a regularization parameter whose value is found from the optimality or quasi-optimality principle.

The freedom in choosing the weights w_1 and w_2 allows us to control the contributions of different sections of the MT curves at different sections of the profile. It is reasonable to increase w_1, w_2 with T (to increase the influence of deep structures) and to take $w_2 > w_1$ (to suppress errors arising in the apparent resistivities because of inaccurate correction for the static shift).

The iteration cycle at level 1 is completed with an approximate solution $\sigma^{TE}(x, z)$ describing the lower part of the geoelectrical model.

Level 2 (the TM inversion)

At this level, inversion of the TM mode is accomplished using transverse ρ_A and φ curves. The main objective of the TM inversion is to evaluate the lithosphere resistance and to optimize conductive sedimentary structures and deep faults. The solution $\sigma^{TE}(x, z)$ obtained in the TE inversion serves as a starting model, stabilizing the TM inversion. Inversion reduces to iterative minimization of the Tikhonov functional

$$\Phi^{TM} = \int_x \int_T w_1(x, T) \left| \ln \frac{\rho_A(3\text{-D, T})}{\rho_A(2\text{-D, TM})} \right|^2 \frac{dT}{T} dx + \int_x \int_T w_2(x, T) |\varphi(3\text{-D, T}) - \varphi(2\text{-D, TM})|^2 \frac{dT}{T} dx + \alpha \int_x \int_z w_3(x, z) |\sigma(x, z) - \sigma^{TE}(x, z)|^2 dz dx, \quad (2)$$

where ρ_A(3-D, T) is the observed value of transverse apparent resistivity corrected for the ρ effect, φ(3-D, T) is the observed value of transverse impedance phase, ρ_A(2-D, TM) and φ(2-D, TM) are the theoretical values of apparent resistivity and phase for the 2-D model $\sigma(x, z)$ excited by a B-polarized field, w_1 and w_2 are weights representing the reliability and informativeness of different sections of the MT curves, w_3 is a weight expressing the degree of confidence in the various elements of the preceding solution $\sigma^{TE}(x, z)$ (the maximum w_3 may be assigned to deep conductive zones in the high-ohmic lithosphere and to resistive structures in the sediments) and α is a regularization parameter whose value is found from the optimality or quasi-optimality principle.

Note that at the level of the TM inversion it is reasonable to increase w_1 and w_2 at high frequencies (to enhance the influence of local shallow structures) and to take $w_2 > w_1$ (to suppress errors arising in the apparent resistivities because of inaccurate correction for the static shift).

The iteration cycle at level 2 is completed with an approximate solution $\sigma^{TM}(x, z)$, which improves the upper part of the geoelectrical model.

The accuracy of the bimodal inversion can be estimated

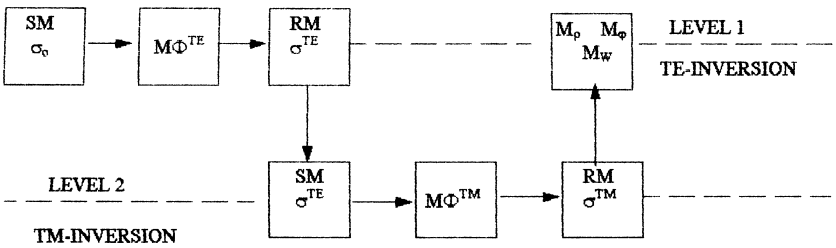

Figure 15. Scheme of the bimodal two-level algorithm: SM, starting model; RM, resulting model; MΦ, minimization of the Tikhonov functional; M, misfit.

from the misfits of the longitudinal resistivities and phases:

$$M_\rho = \int_x \int_T w_1 \left| \ln \frac{\rho_A(\text{3-D, L})}{\rho_A(\text{2-D, TE})} \right|^2 \frac{dT}{T} dx, \quad (3)$$

$$M_\varphi = \int_x \int_T w_2 |\varphi(\text{3-D, L}) - \varphi(\text{2-D, TE})|^2 \frac{dT}{T} dx, \quad (4)$$

where ρ_A(3-D, L) is the observed value of the longitudinal apparent resistivity corrected for the ρ and S effects, φ(3-D, L) is the observed value of the longitudinal impedance phase, ρ_A(2-D, TE) and φ(2-D, TE) are the theoretical values of the apparent resistivity and phase for the 2-D model $\sigma^{TM}(x, z)$ excited by an E-polarized field, and w_1 and w_2 are the same weights as used at level 1.

The misfit of the magnetic field can also be calculated:

$$M_W = \int_x \int_T w_4 |W^\perp(\text{3-D, T}) - W^\perp(\text{2-D, TE})|^2 \frac{dT}{T} dx, \quad (5)$$

where $W^\perp$(3-D, T) is the observed value of the transverse component of the tipper (relating to the transverse component of the horizontal magnetic field), $W^\perp$(2-D, TE) is the theoretical value of the tipper for the 2-D model $\sigma^{TM}(x, z)$ excited by an E-polarized field and w_4 is a weight controlling the magnetic field contribution. The M_W-misfit is very significant, since the low-frequency magnetic field is slightly affected by a near-surface inhomogeneity.

If M_ρ, M_φ and M_W are sufficiently small, the model $\sigma^{TM}(x, z)$ is viewed as the final result of the bimodal inversion. For large M_ρ, M_φ and M_W one can return to level 1 and repeat the iterations, stabilizing the inversion of ρ_A(3-D, L) and φ(3-D, L) by proximity to $\sigma^{TM}(x, z)$. Such an external iterative cycle consists of successive returns to level 1 and transitions to level 2. The iterations are completed when M_ρ, M_φ and M_W are sufficiently small.

Certainly, this algorithm is not universal. It may well change, adapting to the specific features of the geological medium, magnetotelluric field and sounding target [particularly in regions with deep conductive faults crossing the high-ohmic lithosphere (Berdichevsky *et al.* 1996)].

An excellent example of an efficient multilevel bimodal algorithm balancing the contributions of the TM and TE modes, taking account of their informativeness, is given by Banks *et al.* (1996).

In the closing stages of bimodal interpretation one can construct a schematic 3-D model of the region and evaluate (or even correct) the errors caused by 2-D approximation of real 3-D structures. An example of such an estimate has been given by Zhdanov & Spichak (1992).

MAGNETOTELLURIC SOUNDINGS IN THE KIRGHIZ TIEN SHAN

By way of illustration, let us consider the 2-D interpretation of MT soundings which were conducted by the Institute of High Temperatures, Russian Academy of Sciences, in the mountains of the Kirghiz Tien Shan (Trapeznikov *et al.* 1997).

Fig. 16 displays a map of the Kirghiz Tien Shan. The MT sounding sites are located along five submeridional profiles 60–280 km long. More than 100 MT soundings covering a range of periods from 0.1 s to 30 min and several long-period MT soundings with T up to 2–3 hr are available.

Tectonics of Kirghiz Tien Shan

The Kirghiz Tien Shan region is divided into zones of Baikal–Caledonian (northern), Hercynian–Caledonian (central) and Hercynian (southern) orogeny. The boundaries between these zones run along deep faults: the Nikolaev line fault, the Atbashi–Inylchek fault and the Talas–Fergana fault.

The Caledonian and Hercynian folded zones belong to

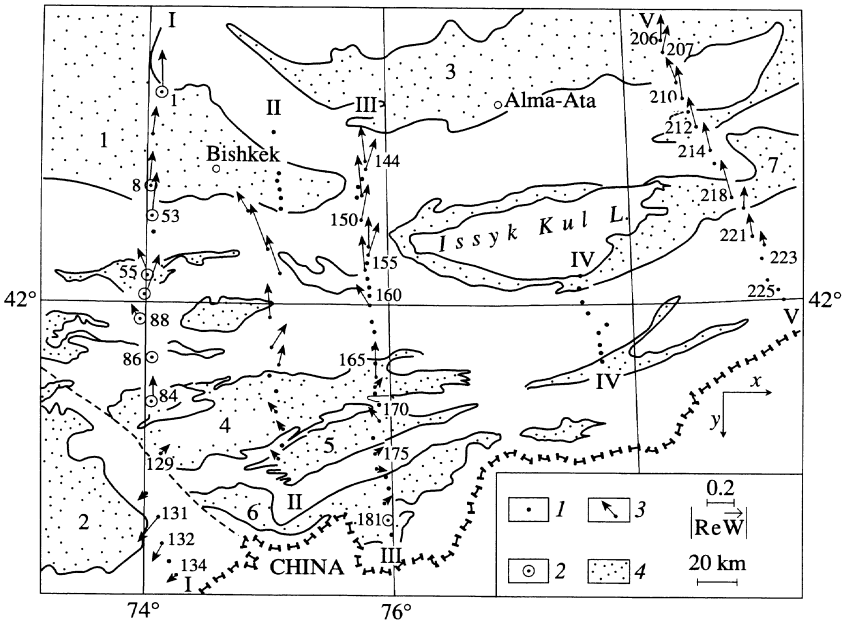

Figure 16. Locations of MT stations in the Kirghiz Tien Shan and induction vectors $\mathscr{R}e\,\mathbf{W}$ at $T = 1600$ s. Numbers in inset: 1, MT sounding sites; 2, long-period deep MT sounding sites; 3, $\mathscr{R}e\,\mathbf{W}$; 4, sedimentary basins, indicated by numbers on main map: Chu (1), Fergana (2), Ili (3), Naryn (4), Atbashi (5), Susamyr (6), Issyk Kul (7).

the Ural–Mongolian geosyncline belt. To the northeast, the Caledonides give way to the Kazakh Shield. To the southeast, the Hercynides are bounded by the ancient Tarim Plate.

The Caledonian and Hercynian structures underwent peneplanation during the Early Mesozoic, and the subsequent tectonic quiet lasted up to the Neogene. The recent mountainous structure of the Tien Shan arose at the site of the post-Palaeozoic peneplain as a result of Alpine movements. The mountains are composed of sedimentary, igneous and metamorphic rocks. The intermontane (Naryn and Issyk Kul) and marginal (Chu and Talas) basins are filled by sediments.

The crustal thickness in the Kirghiz Tien Shan ranges from 40–45 to 60–65 km. Many earthquakes with magnitude up to 6–7 attest to the tectonic activity of the present-day Tien Shan.

Construction of interpretation model

Interpretation of MT soundings begins with the construction of an interpretation model (a compact set of possible solutions). We examine *a priori* information and observation data that can help in constructing the interpretation model.

A priori information

We will proceed from the following known facts: (1) the mountains of the Kirghiz Tien Shan strike sublatitudinally, (2) the Caledonian and Hercynian folding zones are separated by deep sublatitudinal faults, (3) the lower Earth's crust contains a regionally developed layer of low velocity and increased absorption of seismic waves, and (4) in the course of recent tectonic activation of the Tien Shan the temperature at a depth of about 20–30 km reached the threshold of dehydration (550–600 °C).

Long-period apparent resistivity curves

Fig. 17 presents the long-period curves of ρ_{xy} and ρ_{yx}. In relation to the strike of the mountains and faults these curves can be considered as longitudinal (ρ_{xy}) and transverse (ρ_{yx}).

The longitudinal ρ_{xy} curves exhibit a distinct minimum and a clearly outlined descending mantle branch, which is close to the standard ρ_{st} curve (small static shift). It seems that these ρ_{xy} curves are weakly distorted and may be used for some rough 1-D estimates by a rule of thumb method. We can presume that minima of the ρ_{xy} curves are caused by a conductive layer. The layer lies at a depth of about 20–30 km, and its conductance increases from 200–300 S in the north (MTS-1) to 1000–1500 S in the south (MTS-86). It is notable that this crustal conductive layer correlates with the layer of low seismic velocity.

The transverse ρ_{yx} curves are of the same type, but their mantle branches are drastically displaced upwards and downwards from the standard ρ_{st} curve (large static shift), and the crustal conductor is pronounced only in MTS-88, being screened in the other soundings.

Magnetotelluric parameters

These invariant parameters are used to estimate the degree of lateral inhomogeneity of a medium, to localize structures and to establish their dimensionality. We usually employ the following parameters.

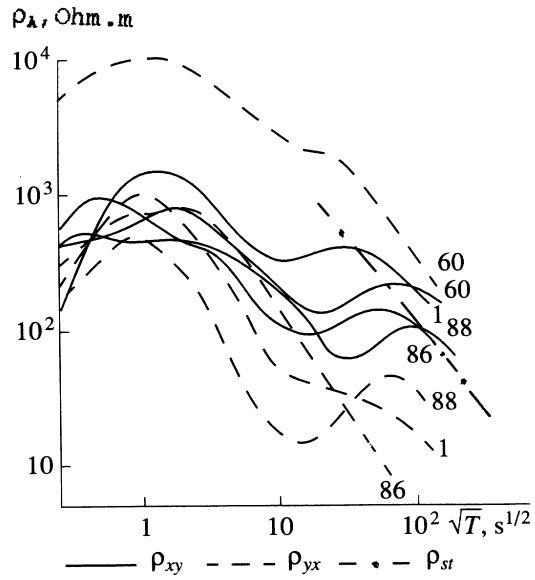

Figure 17. Longitudinal (ρ_{xy}) and transverse (ρ_{yx}) apparent resistivity curves of deep MT soundings; the numbers 1, 60, 86 and 88 indicate the MT sounding sites.

(1) Parameter of inhomogeneity,

$$N = \left| \frac{Z_p^+ - Z_p^-}{Z_p^+ + Z_p^-} \right|, \tag{6}$$

where Z_p^+ and Z_p^- are the principal values of the impedance tensor determined by means of the Eggers eigenstate formulation (Eggers 1982). For laterally homogeneous 1-D media, $N = 0$.

(2) Parameter of asymmetry (Swift 1967),

$$\text{skew} = \left| \frac{Z_{xx} + Z_{yy}}{Z_{xy} - Z_{yx}} \right|, \tag{7}$$

where Z_{xx}, Z_{xy}, Z_{yx}, Z_{yy} are components of the impedance tensor. For 1-D, 2-D and axisymmetric 3-D media, skew = 0.

(3) Angular parameter of asymmetry,

$$A = \left| |\theta_p^+ - \theta_p^-| - \frac{\pi}{2} \right|, \tag{8}$$

where θ_p^+ and θ_p^- are the azimuths of the principal directions of the impedance tensor determined by means of the Eggers eigenstate formulation (Eggers 1982). For 1-D, 2-D and axisymmetric 3-D media, $A = 0$.

(4) Phase-sensitive parameter of asymmetry (Bahr 1988),

$$\eta = \frac{\sqrt{|\mathcal{I}m(Z_{yx}Z_{xx}^* - Z_{xy}Z_{yy}^*)|}}{|Z_{xy} - Z_{yx}|}, \tag{9}$$

where the asterisk indicates the complex conjugate. For a superposition of 2-D regional (deep) and 3-D local (shallow) structures and sufficiently low frequency, $\eta = 0$.

Fig. 18 shows the graphs of magnetotelluric parameters obtained along profile III–III (Fig. 16) at $T = 1600$ s. The values of N almost everywhere exceed 0.3, indicating a strong lateral inhomogeneity of the Earth's crust. The values of A range from a few degrees to a few tens of degrees, suggesting both 2-D and 3-D inhomogeneities. The graph of skew is

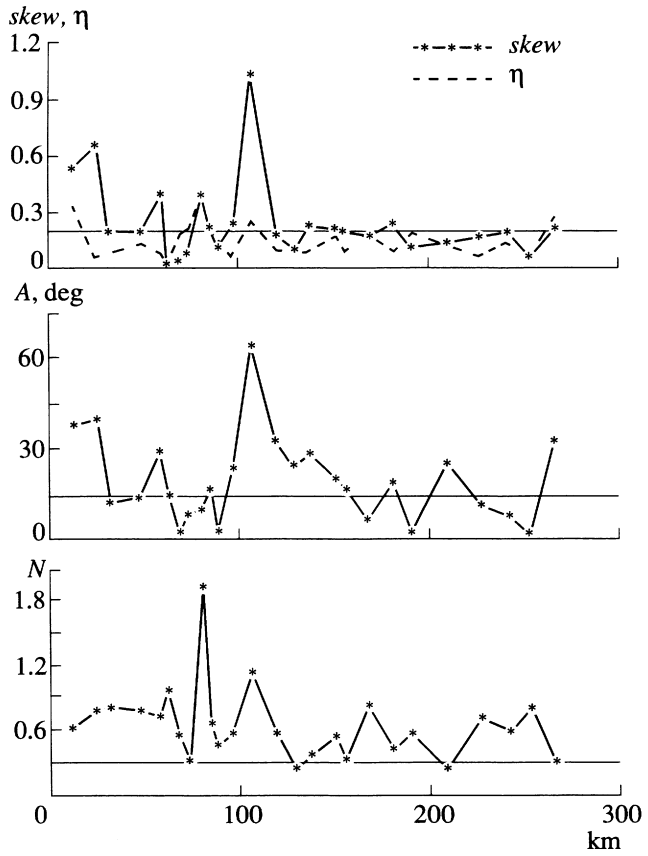

Figure 18. Graphs of magnetotelluric parameters along profile III–III at $T = 1600$ s.

similar to that of A. In some parts of the profile, large values of skew $\gg 0.2$ correlate with relatively small values of η, revealing a superposition of 2-D regional and 3-D local structures. Note that the behaviour of N, A and skew is weakly dependent on frequency. So, we can relate the field distortions to the galvanic effects of a near-surface inhomogeneity.

Polar diagrams of the impedance tensor (Handbook 1989; Berdichevsky, Vanyan & Nguen Tkhan Van 1993)

Polar diagrams of $|Z_{xy}|$, $\arg Z_{xy}$ and $|Z_{yy}|$ typical of the Kirghiz Tien Shan are presented in Fig. 19 (profile III–III, $T = 1600$ s). No regularity can be seen in the behaviour of the amplitude diagrams $|Z_{xy}|$, $|Z_{yy}|$. Their shape and orientation vary chaotically. This points to a strong effect of local 3-D inhomogeneities, producing a random noise. At the same time, the phase diagrams of $\arg Z_{xy}$ in most cases are appreciably elongated in the meridional direction, reflecting the latitudinal strike of the regional 2-D structures.

Principal directions of the impedance tensor

The principal directions of the impedance tensor are plotted in Fig. 20 (profile III–III, $T = 1600$ s). The directions PD_E have been determined as the directions of the major axes of the polarization ellipses of the electric eigenfields in the Eggers eigenstate formulation (Eggers 1982). They vary chaotically, reflecting a random noise caused by local 3-D inhomogeneities. The directions PD_B have been determined as

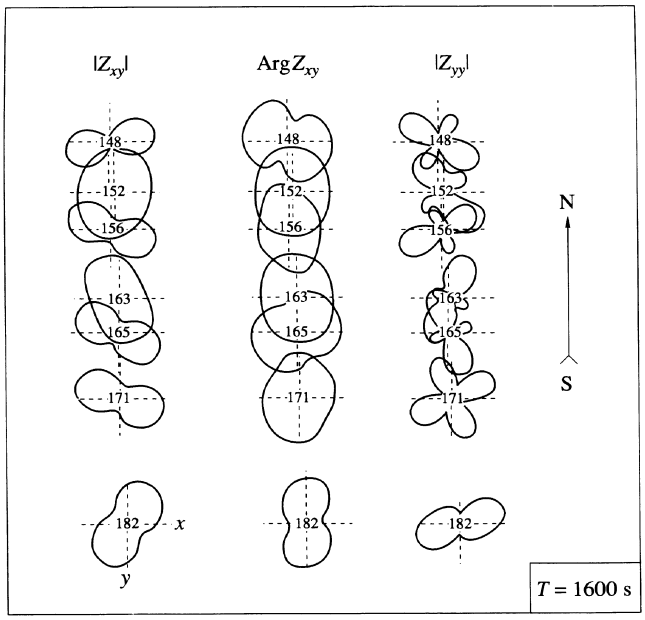

Figure 19. Polar diagrams of the impedance tensor in profile III–III at $T = 1600$ s.

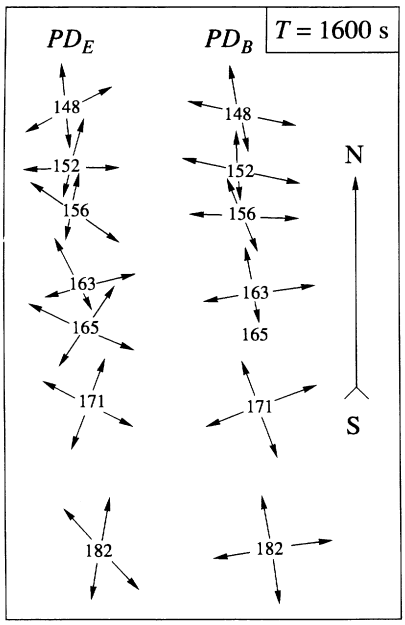

Figure 20. Principal directions of the impedance tensor in profile III–III at $T = 1600$ s.

the principal directions of the 2-D impedance tensor in the Bahr decomposition (Bahr 1988). They gravitate to meridional and latitudinal directions, with rather small fluctuations. The same is observed along profile I–I. Thus, the Bahr decomposition confirms the latitudinal strike of the regional 2-D structures. A similar situation exists along profile V–V, but here the regional structures strike sublatitudinally, with an azimuth of 80°–260°.

Magnetovariation anomalies

Additional geoelectrical information comes from the anomalies of magnetic variations. These anomalies are commonly

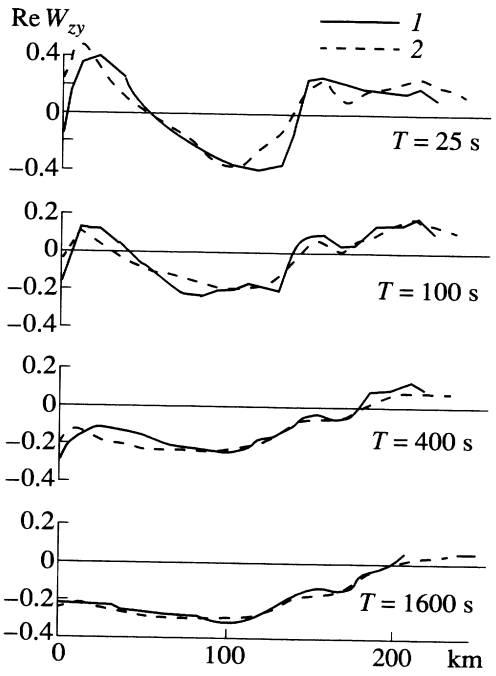

Figure 21. Graphs of $\mathscr{R}e\, W_{zy}$ along profile III–III: 1, observed; 2, computed.

described by the Wiese–Parkinson matrix (also known as Vozoff's tipper) relating the vertical component of the magnetic field to its horizontal components: $H_z = W_{zx}H_x + W_{zy}H_y$ (Berdichevsky & Zhdanov 1984; Vozoff 1991). The components W_{zx}, W_{zy} are used to construct the real and imaginary induction vectors (induction arrows).

Fig. 16 shows the real induction vectors $\mathscr{R}e\,\mathbf{W}$ at $T = 1600$ s. All of the northern part of the Kirghiz Tien Shan (including the Chu and Ili basins) is characterized by large vectors $\mathscr{R}e\,\mathbf{W}$, oriented mostly northwards (profiles I–I and III–III) or northwards–northwestwards (profile V–V). Such a pattern is consistent with the assumption that the conductance of the crustal low-ohmic layer revealed by long-period MT soundings regionally increases in the southward direction.

Now let us turn to Fig. 21, which shows the graphs of $\mathscr{R}e\, W_{zy}$ obtained along profile V–V at $T = 25$, 100, 400 and 1600 s. The regional magnetovariation anomaly caused by the laterally inhomogeneous crustal conductive layer is clearly seen at $T = 1600$ s. A few fairly weak local anomalies correlating with maxima of the parameter N are observed against this background.

With increasing frequency, the regional anomaly decays and the local anomalies build up. They can be associated with deep conductive faults or intermontane sedimentary depressions.

Interpretation model

Summing up, we can construct the interpretation model as a set of 2-D media which include the following elements: (1) a laterally inhomogeneous upper layer (sediments), (2) the high-ohmic crust with vertical conductive channels (faults?), (3) a laterally inhomogeneous conductive layer in the lower crust, (4) the resistive mantle and (5) the conductive mantle (asthenosphere?). The model strikes latitudinally (profiles I–I and III–III) or sublatitudinally (profile V–V).

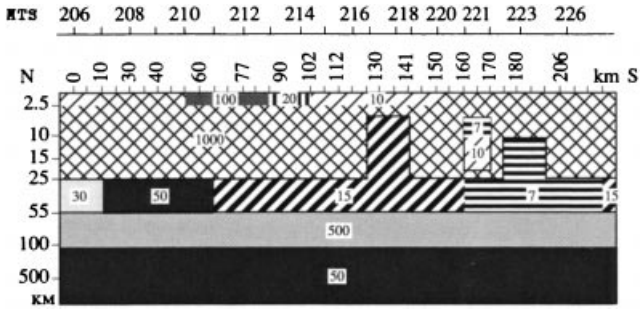

Figure 22. Starting model for profile V–V. The numbers within the model show the resistivities in Ω m.

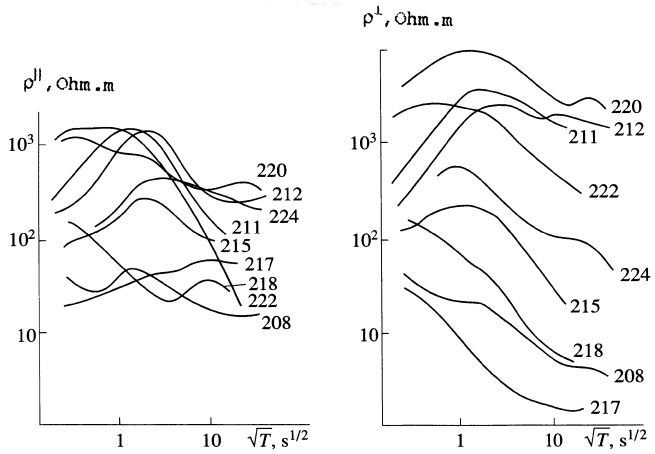

Figure 23. Longitudinal ($\rho^{\parallel}$) and transverse ($\rho^{\perp}$) apparent resistivity curves in profile V–V; the numbers 208–224 indicate the MT sounding sites.

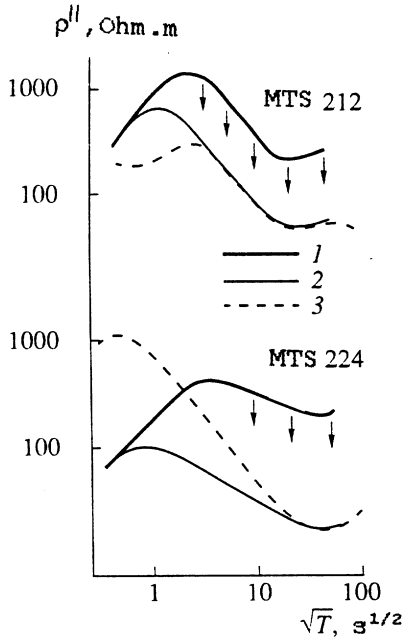

Figure 24. Correction of the $\rho^{\parallel}$ curves for the S effect: 1, observed; 2, corrected; 3, reference (calculated from the starting model). Arrows indicate the displaced portion of the $\rho^{\parallel}$ curves.

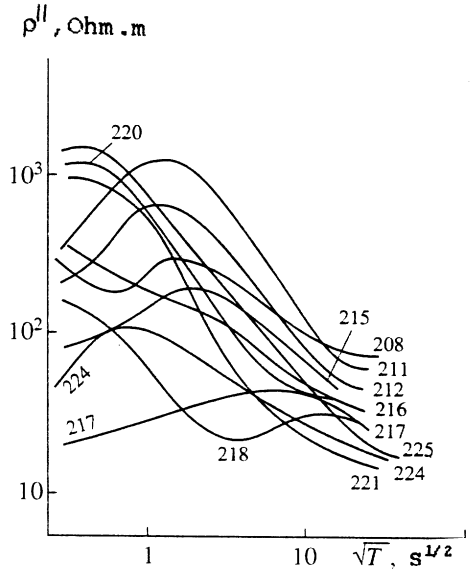

Figure 25. Shift-corrected longitudinal $\rho^{\parallel}$ curves in profile V–V.

Bimodal inversion

Inversion of MT curves should be preceded by the construction of a starting model and corrections for static shift.

Starting model

The starting model has been chosen on the basis of magnetovariation data. Fig. 22 shows the starting model for profile V–V, constructed by means of a trial-and-error method. It contains all elements of the interpretation model and is in good accordance with the behaviour of the tipper (see Fig. 21).

Corrections for static shift

The longitudinal ($\rho^{\parallel}$) and transverse ($\rho^{\perp}$) apparent resistivity curves obtained in profile V–V are presented in Fig. 23. There is no question that not only the transverse $\rho^{\perp}$ curves but also the longitudinal $\rho^{\parallel}$ curves are distorted by a strong static shift. The position of the apparent resistivity curves correlates with changes in the conductance of the sedimentary cover. We can thus relate the observed static shift predominantly to the *S* type. We remove the static shift of the longitudinal $\rho^{\parallel}$ curves by displacing their low-frequency branches to the reference longitudinal $\rho^{\parallel}$ curves calculated from the starting model (Fig. 22). Such a reduction is shown in Fig. 24. The shift-corrected longitudinal $\rho^{\parallel}$ curves are shown in Fig. 25.

TE and TM inversions

Inversion of the longitudinal and transverse ρ_A curves was performed using the two-level bimodal algorithm described

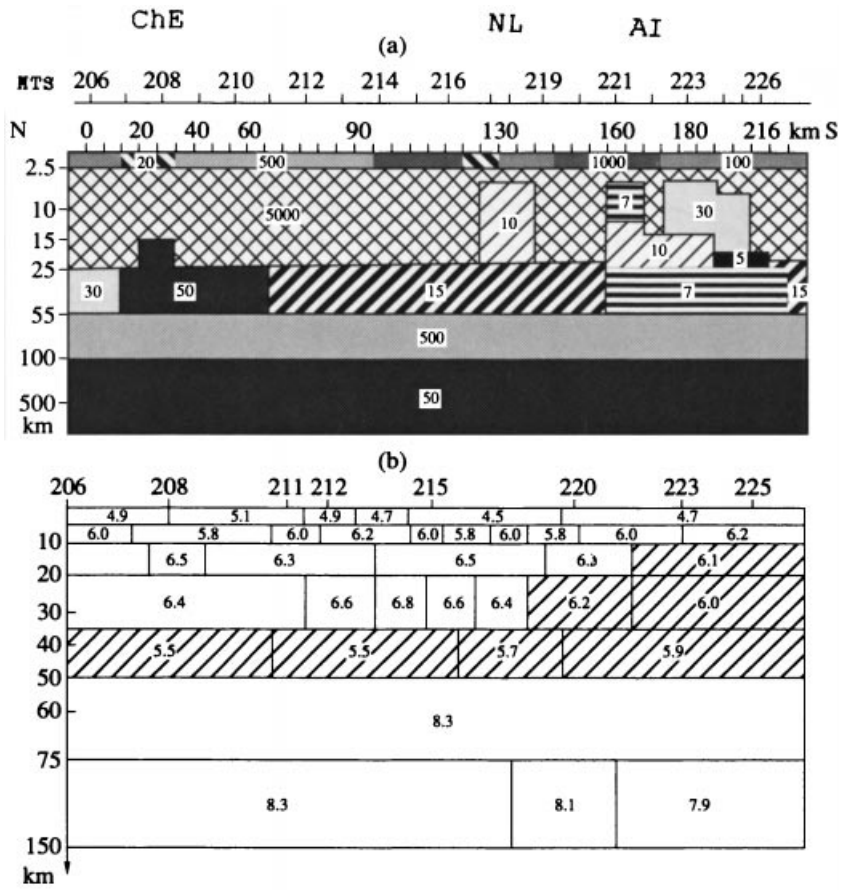

Figure 26. Geoelectric and velocity cross-sections in profile V–V. (a) Geoelectric model from inversion of the $\rho^{\parallel}$ and $\rho^{\perp}$ curves; the numbers within the model show the resistivities in Ω m; ChE, Chilik earthquake zone; NL, fault zone of the Nikolaev line; AI, Atbashi–Inylchek fault zone. (b) Velocity model from seismic tomography; the numbers within the model show velocities in km s^{-1}; low-velocity zones are hatched.

earlier in this paper (Fig. 15). Minimization of the misfits was carried out by means of a quasi-1-D optimization technique which reduces the 2-D inversion to an iterative sequence of 1-D inversions corrected by taking account of 2-D effects (Dmitriev 1987; Oldenburg & Ellis 1993). At level 1, the TE inversion specified and detailed conductive zones in the middle and upper crust. At level 2, the TM inversion helped in evaluating the resistance of the high-ohmic crust and differentiating the sedimentary cover. It was the TM inversion which showed that conductive channels in the fault zones do not reach the sedimentary cover. The bimodal inversion resulted in the model which is shown in Fig. 26a. The model gives pseudo-sections of the apparent resistivites and tipper that conform fairly well to the pseudo-sections of these characteristics derived directly from the observed data (Fig. 27). It is obvious that elimination of one of the modes strips information from or even destroys the model obtained.

The stability of the model was examined in a series of computing experiments. In particular, it was shown that the substitution of longitudinal phase curves for the shift-corrected apparent resistivity curves scarcely affects the results of the bimodal inversion. This suggests that inaccuracy in the static shift corrections of the $\rho^{\parallel}$ curves did not introduce large errors into the final model.

Consider the geoelectrical model obtained. In the lower crust, at depths of 25–55 km, we clearly see the conductive layer, whose resistivity increases from 7–15 to 30–300 Ω m in a northerly direction. The upper crust is high-ohmic (5000 Ω m and more). It contains local vertical conductive zones that correlate with the faults of the Nikolaev line and the Atbashi–Inylchek zone. These zones branch out from the crustal conductive layer and reach depths of about 3–8 km. In the north, in the Chilik earthquake zone, a ledge of crustal conductive layer is observed.

On the nature of crustal conductors

Fig. 26b presents a velocity model constructed from seismic tomography data (Roecker *et al.* 1993). The agreement between the geoelectric and seismic cross-sections catches the eye. The

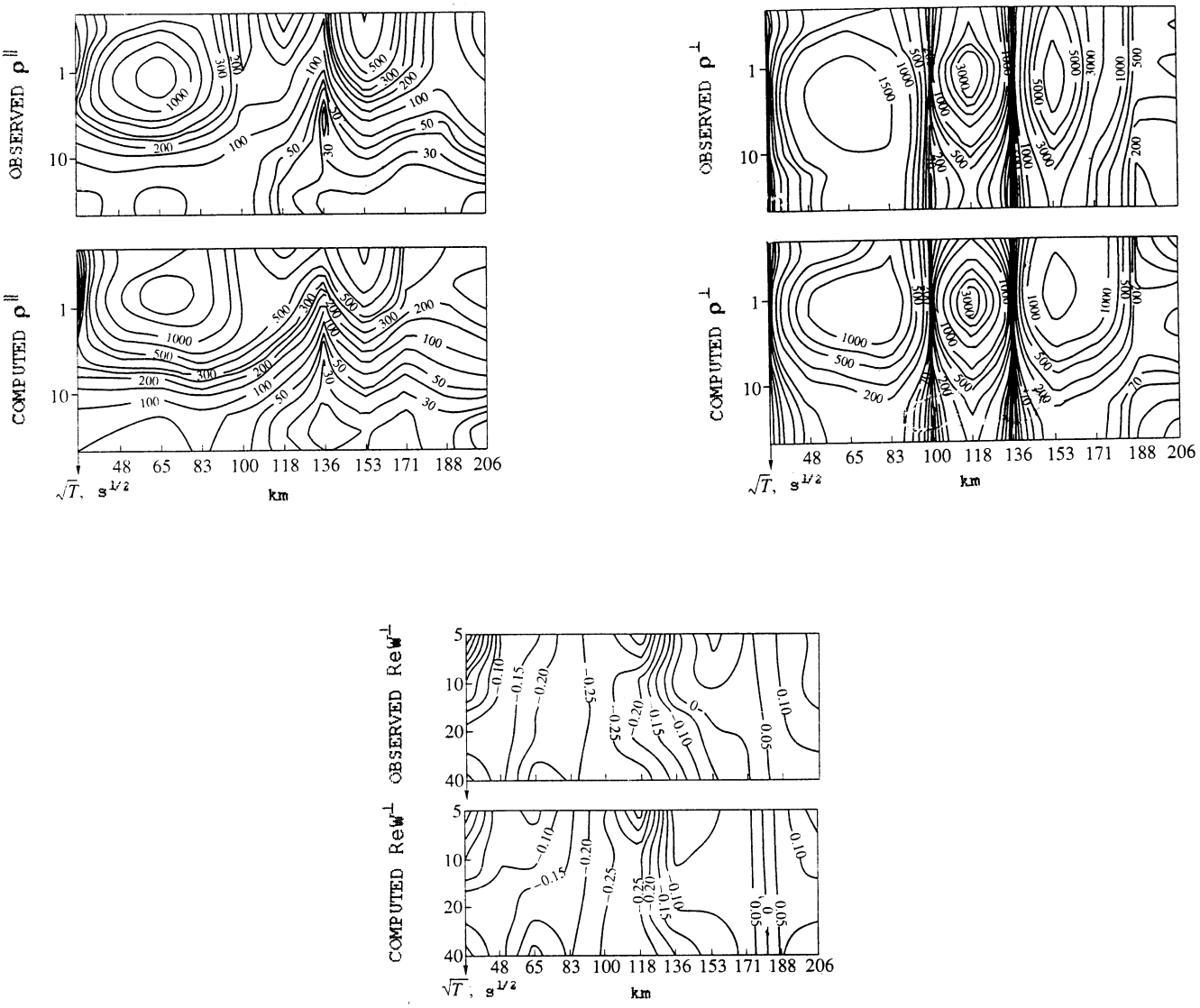

Figure 27. Pseudo-sections of observed and computed values of $\rho^{\parallel}$, $\rho^{\perp}$ and $\mathscr{R}e\, W^{\perp}$ in profile V–V.

conductive layer in the lower crust is associated with a layer of low velocity $V_P = 5.5$–5.9 km s^{-1}, and the Atbashi–Inylchek conductive zone in the upper crust is manifested as a zone of low velocity $V_P = 6.0$–6.2 km s^{-1}. Note also that the conductive ledge in the Chilik earthquake zone correlates with a zone of enhanced seismic absorption (Kvetinsky *et al.* 1993) and geothermic anomaly.

The stable relationship between conductors and low seismic velocity (and enhanced seismic absorption) favours the fluid explanation of the crustal electrical conductivity. Thus, we may state fairly certainly that fault zones and deep horizons in the crust are saturated with fluids. There is good reason to believe that it is the dehydration during recent activation of the Kirghiz Tien Shan that has generated the fluids. Estimates show that a poor penetrability of the upper crust enabled the fluids to exist throughout the activation period, up to the present. The fluids are partly replaced only through the fault zones. In the context of this picture, the question of carbon liberation does not arise.

CONCLUSIONS

Concluding, we would like to stress two main points.

(1) The TM and TE modes of the 2-D magnetotelluric field satisfy the principle of information complementarity.

(2) The most reliable and comprehensive information on the Earth's conductivity can be obtained by means of a bimodal interpretation of the MT data, using both modes.

ACKNOWLEDGMENTS

We are grateful to L. Vanyan, I. Varentsov, S. Park and J. Booker for many valuable discussions and constructive criticisms. We especially thank P. Wannamaker and S. Park for reading the paper and making helpful comments. We express our gratitude to P. Wannamaker for control calculation of some models described in the paper.

This research was supported by Russian Foundation of Fundamental Investigations, Project code 96-05-64340.

REFERENCES

Alperovich, I.M., Kononov, V.E., Nikiforov, V.M., Sludnev, Ju.G. & Kharakhinov, V.V., 1980. Structure of the islands Sakhalin and Iturup according MT-data, in *Deep Eelectromagnetic Soundings on the Far East,* Far East Scientific Centre, Vladivostok.

Bahr, K., 1988. Interpretation of magnetotelluric impedance tensor: regional induction and local telluric distortion, *J. Geophys.,* **62,** 119–127.

Banks, R. I., Livelybrooks, D., Jones, P. & Longstaff, R., 1996. Causes of high crustal conductivity beneath the Iapetus suture zone in Great Britain, *Geophys. J. Int.,* **124,** 433–455.

Berdichevsky, M.N. & Dmitriev, V.I., 1976a. Basic principles of interpretation of magnetotelluric sounding curves, in *Geoelectric and Geothermal Studies,* Akademiai Kiado, Budapest.

Berdichevsky, M.N. & Dmitriev, V.I., 1976b. Distortions of magnetic and electrical fields by near-surface lateral inhomogeneities, *Acta Geodaet., Geophys., et Montanist., Acad. Sci. Hung.,* **11,** 447–483.

Berdichevsky, M.N. & Jakovlev, A.G., 1990. Analytical model of magnetotelluric sounding distorted by screening effect, *Phys. solid Earth,* **26,** 520–524.

Berdichevsky, M.N. & Kulikov, V.A., 1994. Sensitivity of deep magnetotelluric sounding in the presence of fluidized faults, *Phys. Earth (Fizika Zemli),* No. 6, 39–49.

Berdichevsky, M.N. & Pokhotelov, D.O., 1996. Violation of dispersion relation between apparent resistivities and impedance phases in 3D-models, in *Proc. 13th Workshop on EM induction in the Earth,* Hokkaido, Japan, p. XX.

Berdichevsky, M.N. & Zhdanov M.S., 1984. *Advanced Theory of Deep Geomagnetic Sounding,* Elsevier, Amsterdam.

Berdichevsky, M.N., Vanyan, L.L., Kuznetsov, V.A., Levadny, V.T., Mandelbaum, M.M., Nechaeva, G.P., Okulessky, B.A., Shilovsky, P.P. & Shpak, I.P., 1980. Geoelectric model of the Baikal region, *Phys. Earth planet. Inter.,* **22,** 1–11.

Berdichevsky, M.N., Dmitriev, V.I., Feldman, I.S., Beresina, N.I., Demidov, A.I. & Jakovlev, S.P., 1988. Interpretation of deep MT-soundings in the Tungus syneclise, *Phys. Earth (Fizika Zemli),* No. 7, 73–79.

Berdichevsky, M.N., Vanyan, L.L. & Dmitriev, V.I., 1989. Methods used in the USSR to reduce near-surface inhomogeneity effects on deep magnetotelluric soundings, *Phys. Earth planet. Inter.,* **53,** 194–206.

Berdichevsky, M.N., Koldayev, D.S. & Jakovlev, A.G., 1992. Magnetotelluric sounding on an ocean coast, *Phys. solid Earth,* **28,** 523–530.

Berdichevsky, M.N., Dmitriev, V.I. & Kulikov, V.A., 1993. On normalization of magnetotelluric field by fluidized faults, *Phys. Earth (Fizika Zemli),* No. 11, 45–54.

Berdichevsky, M.N., Vanyan, L.L. & Nguen Tkhan Van, 1993. Phase polar diagrams of the magnetotelluric impedance, *Phys. Earth (Fizika Zemli),* No. 2, 19–23.

Berdichevsky, M.N., Dmitriev, V.I. & Kulikov, V.A., 1994. Magnetotelluric sounding in the presence of fluidized faults, in *Proc. XII workshop on EM induction in the Earth,* IAGA, Brest.

Berdichevsky, M.N., Dmitriev, V.I. & Kuznetsov, V.A., 1995. Bimodal two-dimensional interpretation of MT-soundings, *Phys. Earth (Fizika Zemli),* No. 10, 15–31.

Berdichevsky, M.N., Borisova, V.P., Golubtsova, N.S., Ingerov, A.I., Konovalov, Yu.F., Kulikov, A.V., Solodilov, L.N., Chernyavsky, G.A. & Shpak, I.P., 1996. Interpretation of magnetotelluric soundings in the Lesser Caucasus, *Phys. solid Earth,* **32,** 352–368.

Bostick, F.X., 1986. Electromagnetic array profiling (EMAP), in *Proc. 56th Ann. Int. SEG Meeting,* Houston, TX.

Dmitriev, V.I., 1987. Inverse problems in electrodynamic prospecting, in *Ill-posed Problems in the Natural Sciences,* Mir, Moscow.

Dmitriev, V.I. & Berdichevsky, M.N., 1988. Statistical model of the *S*-effect, *Proc. IX Workshop on EM induction in the Earth,* IAGA, Sochi.

Dmitriev, V.I. & Pozdnjakova, E.E., 1991. Mathematical modeling of low-frequency electromagnetic fields in three-dimensional medium, in *Forward and Inverse Problems of Mathematical Physics, Proceedings of Computing Mathematics and Cybernetics Department of Moscow State University,* pp. 139–151.

Dmitriev, V.I., Berdichevsky, M.N., Barashkov, I.S., Lebedeva, N.A. & Nechaeva, G.P., 1982. On the influence of deep faults on resolving power of magnetotelluric sounding, *Phys. Earth (Fizika Zemli),* No. 8, 100–102.

Dyakonova, A.G., Ingerov, A.I. & Rokityansky, I.I., 1986. *Electromagnetic Soundings on the Eastern-European Platform and in the Urals,* Naukova Dumka, Kiev.

Eggers, D.E., 1982. An eigenstate formulation of the magnetotelluric impedance tensor, *Geophysics,* **47,** 1204–1214

Fainberg, E.B., 1983. Global geomagnetic sounding, in *Mathematical Modeling of Electromagnetic Fields,* Izmiran, Moscow.

Fainberg, E.B., Andrieux, P., Guerin, R. & Poltoratskaya, O.L., 1995. Dynamic correction of amplitude curves of magnetotelluric sounding distorted by the influence of near-surface inhomogeneities, *Phys. Earth (Fizika Zemli),* No. 7, 29–34.

Fischer, G. & Schnegg, P., 1993. The magnetotelluric dispersion relations over 2-D structures, *Geophys. J. Int.,* **115,** 1119–1123.

Golubev, N.G. & Varentsov, I.M., 1994. MT-data inversion: stable optimization methods and interactive graphics, *Proc. XII Workshop on EM induction in the Earth,* IAGA, Brest.

Gupta, C.J. & Jones, A.G., 1995. Electrical conductivity structure of the Purcell Anticlinorium in southeast British Columbia and northwest Montana, *Can. J. Earth Sci.,* **32,** 1564–1583.

Handbook of the Geophysicist, 1989. Vol. 1, *Magnetotelluric method,* Nedra, Moscow.

Ingham, M., 1996. Magnetotelluric soundings across the South Island of New Zealand: electrical structure associated with the orogen of the Southern Alps, *Geophys. J. Int.,* **124,** 134–148.

Jones, A.G., 1988. Static shift of magnetotelluric data and its removal in a sedimentary basin enviroment, *Geophysics,* **53,** No. 7, 967–978.

Jupp, D.L.B. & Vozoff, K., 1977. Two-dimensional magnetotelluric inversion, *Geophys. J. R. astr. Soc.,* **50,** 333–352.

Kaufman, A.A., 1974. *Basic Theory of Inductive Mineral Prospecting,* Nauka, Novosibirsk.

Kaufman, A.A., 1988. Reduction of the geological noise in magnetotelluric sounding, *Geoexploration,* **25,** 145–161.

Kaufman, A.A. & Keller, G.V., 1981. *The Magnetotelluric Sounding Method,* Elsevier, Amsterdam.

Kovtun, A.A., 1989. Structure of the Earth's crust and upper mantle on the North-West of Eastern-European platform according to MT-data, Leningrad University Press, Leningrad.

Kovtun, A.A. & Vardanyants, I.L., 1985. Models of crustal conductive zones on the northwest of the Russian platform, in *Electromagnetic Soundings of the Earth,* Izmiran, Moscow.

Kvetinsky, S.G., Kopnichev, Y.F., Mikhaylova, I.I., Nurmagambetov, A.N. & Rakhmatullin, M.Kh., 1993. Inhomogeneities of lithosphere and asthenosphere in focus zones of strong earthquakes in the Northern Tien Shan, *Doklady AN SSSR,* **329,** 25–28.

Mackie, R.L., Bennet, B.R. & Madden, T.R., 1988. Long-period magnetotelluric measurements near the central California coast, *Geophys. J. Int.,* **95,** 181–194.

Moroz, Ju.F., 1991. *Electrical Conductivity of the Earth's Crust and Upper Mantle of Kamchatka,* Nauka, Moscow.

Oldenburg, D.W. & Ellis, R.G., 1993. Efficient inversion of magnetotelluric data in two dimensions, *Phys. Earth planet. Inter.,* **81,** 177–200.

Park, S.K., 1985. Distortion of magnetotelluric sounding curves by three-dimensional structures, *Geophysics,* **50,** 785–797.

Park, S.K., 1996. Magnetotelluric studies, in *Geodynamics of Intracontinental Mountain Building in the Tien Shan,* proposal to the National Science Foundation, pp. 22–23.

Park, S.K., Orange, A.S. & Madden, T.D., 1983. Effects of three-dimensional structure on magnetotelluric sounding curves, *Geophysics,* **48,** 1402–1405.

Park, S.K., Biasi, G.P., Mackie, R.L. & Madden, T.R., 1991. Magnetotelluric evidence for crustal suture zones bounding the southern Great Valley, California, *J. geophys. Res.,* **96,** 353–376.

Pellerin, L. & Hohmann, G.W., 1990. Transient electromagnetic inversion: a remedy for magnetotelluric static shift, *Geophysics,* **55,** 1242–1250.

Roecker, S.W., Sabitova, T.M., Vinnik, L.P., Burmakov, Y.A., Golvanov, M.I., Mamatkhanova, R. & Munirova, L., 1993. Three-dimensional elastic wave velocity structure of western and central Tien Shan, *J. geophys. Res.,* **98,** 15 779–15 795.

Rokityansky, I.I., 1982. *Geoelectromagnetic Ivestigation of the Earth's Crust and Mantle,* Springer, Berlin.

Semenov, V.Yu., Ernst, T., Jozwiak, W. & Pawliszyn, J., 1993. The crust and mantle electrical conductivity estimation using Polish observatory data, *Acta Geophys. Pol.,* **41,** 375–384.

Sternberg, B.K., Washburne, J.C. & Pellerin, L., 1988. Correction for the static shift in magnetotellurics using transient electromagnetic sounding, *Geophysics,* **53,** 1459–1468.

Svetov, B.S., 1973. *Theory, Methodology, and Interpretation in Low-frequency Inductive Prospecting,* Nedra, Moscow.

Swift, C.M., 1967. A magnetotelluric investigation of an electrical conductivity anomaly in the southwestern United States, *PhD thesis,* MIT, Cambridge, MA.

Tikhonov, A.N. & Arsenin, V.Ya., 1977. *Solutions of Ill-Posed Problems,* Wiley, New York.

Torres-Verdin, C. & Bostick, F.X., 1992. Principles of spatial surface electric field filtering in magnetotellurics: electromagnetic array profiling, *Geophysics,* **57,** 603–622.

Trapeznikov, Yu.A., Andreeva, E.V., Batalev, V.Yu., Berdichevsky, M.N., Vanyan, L.L., Volykhin, A.M., Golubtsova, N.S. & Rybin, A.K., 1997. Magnetotelluric soundings in the Kyrgyz Tien Shan, *Phys. solid Earth,* **33,** 1–17.

Veselovsky, V.V. & Yudin, M.N., 1988. On sufficient condition of two-dimensionality in MTS, *Phys. Earth (Fizika Zemli),* No. 4, 103–108.

Vozoff, K., 1991. The magnetotelluric method, in *Electromagnetic Methods in Applied Geophysics—Applications,* Vol. 2, Society for Exploratory Geophysics, Tulsa.

Wannamaker, P.E., Hohman, G.W. & Ward, S.H., 1984. Magnetotelluric responses of three-dimensional bodies in layered earth, *Geophysics,* **49,** 1517–1533.

Wannamaker, P.E., Stodt, J.A. & Rijo, L., 1987. A stable finite element solution for two-dimensional magnetotelluric modelling, *Geophys. J. R. astr. Soc.,* **88,** 277–296.

Wannamaker, P.E., Booker, J.R., Jones, A.G., Chave, A.D., Filloux, J.H., Waff, H.S. & Law, L.K., 1989. Resistivity cross-section through the Juan de Fuca subduction system and its tectonic implication, *J. geophys. Res.,* **94,** 14 127–14 144.

Wannamaker, P.E., Wright, P.M., Zhou Zi-xing, Li Xing-bin & Zhao Jing-xiang, 1991. Magnetotelluric transect of Long Valley caldera: resistivity cross-section, structural implications, and the limits of a 2-D analysis, *Geophysics,* **56,** 926–940.

Weaver, J.T., 1994. *Mathematical Methods for Geo-electromagnetic Induction,* Research Studies Press, Taunton; Wiley, New York, NY.

Zhdanov, M.S. & Keller, G.V. 1994. *The Geoelectrical Methods in Geophysical Exploration,* Elsevier, Amsterdam.

Zhdanov, M.S. & Spichak, V.V., 1992. *Mathematical Modeling of Electromagnetic Field in Three-dimensional Media,* Nauka, Moscow.

Zinger, B.Sh., 1992. Correction for distortions of magnetotelluric fields: limits of validity and static approach, *Surv. Geophys.,* **13,** 309–340.